Sensitivity of the Ocean's Climate to Diapycnal Diffusivity in an EMIC. Part I: Equilibrium State

FABIO DALAN AND PETER H. STONE

Joint Program on the Science and the Policy of Climate Change, Massachusetts Institute of Technology, Cambridge, Massachusetts

IGOR V. KAMENKOVICH

Joint Institute for the Study of the Atmosphere and the Oceans, University of Washington, Seattle, Washington

JEFFERY R. SCOTT

Joint Program on the Science and the Policy of Climate Change, Massachusetts Institute of Technology, Cambridge, Massachusetts

(Manuscript received 9 April 2004, in final form 15 December 2004)

ABSTRACT

The diapycnal diffusivity in the ocean is one of the least known parameters in current climate models. Measurements of this diffusivity are sparse and insufficient for compiling a global map. Inferences from inverse methods and energy budget calculations suggest as much as a factor of 5 difference in the global mean value of the diapycnal diffusivity. Yet, the climate is extremely sensitive to the diapycnal diffusivity. In this paper the sensitivity of the current climate to the diapycnal diffusivity is studied, focusing on the changes occurring in the ocean circulation. To this end, a coupled model with a three-dimensional ocean with idealized geometry is used.

The results show that, at equilibrium, the strength of the thermohaline circulation in the North Atlantic scales with the 0.44 power of the diapycnal diffusivity, in contrast to the theoretical value based on scaling arguments for uncoupled models of 2/3. On the other hand, the strength of the circulation in the South Pacific scales with the 0.63 power of the diapycnal diffusivity in closer accordance with the theoretical value.

The vertical heat balance in the global ocean is controlled by, in the downward direction, (i) advection and (ii) diapycnal diffusion; in the upward direction, (iii) isopycnal diffusion and (iv) parameterized mesoscale eddy [Gent–McWilliams (GM)] advection. The size of the latter three fluxes increases with diapycnal diffusivity, because the thickness of the thermocline also increases with diapycnal diffusivity leading to greater isopycnal slopes at high latitudes, and hence, enhanced isopycnal diffusion and GM advection. Thus larger diapycnal diffusion is compensated for by changes in isopycnal diffusion and GM advection. Little change is found for the advective flux because of compensation between downward and upward advection.

Sensitivity results are presented for the hysteresis curve of the thermohaline circulation. The stability of the climate system to slow freshwater perturbations is reduced as a consequence of a smaller diapycnal diffusivity. This result is consistent with the findings of two-dimensional climate models. However, contrary to the results of these studies, a common threshold for the shutdown of the thermohaline circulation is not found in this model.

1. Introduction

The diapycnal turbulent mixing of heat and salt in the ocean is commonly associated with internal waves, primarily generated by interaction of tides with topography at the bottom of the ocean and wind stirring at its surface. Diapycnal mixing is important for the global energy balance, and in numerical models, is represented by the vertical diffusion. The equilibrium state of the global ocean circulation is very sensitive to the value and the location of the diapycnal diffusivity (e.g., Bryan 1987; Cummins et al. 1990; Scott and Marotzke 2002). Yet, a global map of the diapycnal diffusivity, based on observations, is not available. Measurements are sparse in space and time, ranging from 5 $cm^2\,s^{-1}$ above the midocean ridge to 0.1 $cm^2\,s^{-1}$ over smooth

Corresponding author address: Fabio Dalan, Via Cavour 44/e, 35030 Rubano (PD), Italy.
E-mail: fabio.dalan@alum.mit.edu

topography (Polzin et al. 1997) and in the thermocline (Ledwell et al. 2000). Inference from the density structure of the global ocean suggests that the global average diapycnal diffusivity is of the order of 1 $cm^2 s^{-1}$, assuming constant upwelling velocity (Munk 1966; Munk and Wunsch 1998), down to 0.2 $cm^2 s^{-1}$, assuming constant energy (mainly tidal) dissipation (Huang 1999). Still, ocean general circulation models (GCMs) use values for the diapycnal diffusivity ranging over an interval larger than the one given from measurements and calculations.[1] Several properties of the climate system are potentially affected by the diapycnal diffusivity. We focus our attention on the scaling behavior of the thermohaline circulation (THC) and the ocean heat transport, the vertical heat balance in the ocean, and the stability of the climate under a quasi-static freshwater perturbation.

The sensitivity of the present ocean circulation to the diapyncal diffusivity has been previously studied in both single-basin and global ocean GCMs. The THC is most sensitive to diapycnal diffusivity in the tropical thermocline (Scott and Marotzke 2002), particularly near the base of the thermocline (Cummins et al. 1990; Bugnion et al. 2004a). Scott and Marotzke's results suggest that enhanced or weakened mixing (via changes in diapycnal diffusivity) below the thermocline affects the deep ocean circulation, with minimal impact on upper ocean properties and ocean heat transport. Although GCM results suggest that the THC also shows a sensitivity to mixing on lateral boundaries versus ocean interior (Scott and Marotzke 2002), to lowest order it is the amount of area-integrated mixing in low latitudes that is the critical quantity helping to drive the meridional overturning (see also Samelson 1998). It is less clear if there is dynamical significance to low-latitude mixing in a basin with active deep-sinking present or one without. For simplicity and to aid in our understanding of numerical results, however, all runs here use uniform diffusivity, in both the horizontal and vertical, and constant in time.

The sensitivity of the THC strength to the diapycnal diffusivity has been examined in single-hemisphere uncoupled OGCMs with idealized topography (Bryan 1987; Marotzke 1997; Park and Bryan 2000; Scott 2000). A simple scaling argument, based on the application of advective–diffusive balance and thermal wind (Welander 1971) is in close agreement with the results from these simple models. Marotzke (1997) and Marotzke and Klinger (2000) present theories for predicting the overturning strength in uncoupled models in a single hemisphere and (closed) single basin, respectively. Gnanadesikan (1999) derives a cubic equation that relates pycnocline depth (and hence overturning strength), which includes the effect of wind forcing and diapycnal mixing for a single basin configuration with a southern channel. However, the scaling behavior of the overturning circulation in a multibasin configuration or in coupled models is largely untested and its dynamics is poorly understood. Here, we show scaling results using our two-basin, coupled configuration, discussing our results in the context of the simple idealized OGCM studies. We also diagnose heat transport in our two-basin model, again comparing our results with those of the documented idealized OGCM studies. We note that the latitudinal temperature contrast in the scaling analyses is treated as an external parameter, but in a coupled model it is not. Since the scaling analyses yield the result that the strength of the overturning and its heat transport increase if either the diapycnal diffusivity or the temperature contrast increases, one would expect in a coupled model that as the diffusivity increases the temperature contrast will decrease, and thus the strength and heat transport of the circulation in a coupled model will not increase with the diapycnal diffusion as rapidly as it does in the scaling analyses.

The analysis of the vertical heat balance in the ocean is a very useful tool for understanding ocean heat uptake and therefore ocean dynamics and thermodynamics. The sensitivity of such balance at equilibrium indicates whether the relative magnitude of the processes transporting heat vertically depends on the diapycnal diffusion. A forthcoming paper (Dalan et al. 2005) will address the question of whether the heat uptake in global warming experiments depends on the diapycnal diffusion.

Gregory (2000) analyzed the heat balance of the vertical fluxes both at equilibrium and in a global warming experiment. He combined together the advective fluxes (Eulerian and parameterized eddy advection) and the diffusive fluxes (isopycnal and diapycnal) when analyzing the global ocean balance. Investigating the balance for different latitude bands and basins, he limited the analysis to a single depth level (160 m). The heat balance at every depth level is presented by Huang et al. (2003). However, he also lumped together the isopycnal diffusive flux and the bolus velocity [Gent–McWilliams (GM)] advective flux.

The ocean's possible equilibrium states are explored in hysteresis experiments where the freshwater flux in

[1] This is according to CMIP2 (Coupled Model Intercomparison Project; see online at see http://www-pcmdi.llnl.gov/cmip/cmiphome.html) documentation—for example, the Australian model from the Bureau of Meteorology Research Center assumes a constant diapycnal diffusivity of 20 $cm^2 s^{-1}$.

the Atlantic Ocean increases (decreases) until the shutdown (recovery) of the THC is reached. The magnitude of freshwater flux increment is made small enough so that the state of the model is always near the equilibrium. Hysteresis experiments tell us how far the equilibrium climate of a model is from the collapse of the THC due to enhanced freshwater flux in the North Atlantic.

Ganopolsky et al. (2001) and Schmittner and Weaver (2001) suggested that the stability of the climate system is reduced for a reduction in vertical diffusivity; that is, the collapse of the circulation is achieved at a smaller freshwater perturbation for small values of the vertical diffusivity. Schmittner and Weaver (2001) noticed also that a common threshold of a minimum THC strength seems to exist, below which the circulation collapses. These results may be biased by the use of models with 2D ocean basins. Such models differ substantially from a 3D ocean model in several aspects, among which are the need to parameterize the effect of rotation and the neglect of zonal variations in the North Atlantic. In 2D ocean models, important processes like convection and downward advection occur at the same location, while in 3D ocean models with idealized topography, they can occur at opposite sides of the Atlantic basin (Marotzke and Scott 1999). Recently, a study with a 3D OGCM (Prange et al. 2003, their Fig. 6) with linearized dynamics confirmed the early collapse of the THC with decreasing vertical mixing but no common threshold was observed.

In analyzing the sensitivity of the current climate to changes in diapycnal diffusivity, we will investigate the power-law relation of the THC and the ocean heat transport in the context of a coupled model with a 3D ocean component. We perform an analysis of the vertical heat balance for the current climate, dividing the heat fluxes into *all* its components, and we study the sensitivity of the vertical heat balance at every depth to changes in diapycnal diffusivity. Last, we perform a sensitivity study of the hysteresis curve to diapycnal diffusivity, using a coupled model that includes a 3D ocean component and the full nonlinear momentum equations.

The paper is organized as follows. In section 2 we describe the numerical model. Section 3 contains the analysis of the equilibrium ocean circulation: here, the scaling behavior of the THC strength and the ocean heat transport is presented; section 4 illustrates the sensitivity of the vertical heat balance in the ocean to the diapycnal diffusivity and in section 5 the same sensitivity is presented for the hysteresis cycle of the THC. Finally, section 6 contains the conclusions.

2. MIT earth model of intermediate complexity

More details about the model can be found in Kamenkovich et al. (2000, 2002).

a. Atmospheric component

The two-dimensional zonally averaged statistical-dynamical atmospheric model was developed by Sokolov and Stone (1998) on the basis of the Goddard Institute for Space Studies (GISS) GCM (Hansen et al. 1983). The model solves the zonally averaged primitive equations in latitude-pressure coordinates. The grid of the model consists of 24 points in the meridional direction, corresponding to a resolution of 7.826°, and nine layers in the vertical. In addition to the parameterizations used in the GCM, the model includes the parameterization of heat, moisture, and momentum transports by large-scale eddies (Stone and Yao 1990). It has a complete moisture and momentum cycle.

Most of the physics and parameterizations of the atmospheric model derive from the GISS GCM. The 2D model, as well as the GISS GCM, allows four different types of surfaces in the same grid cell, namely open ocean, sea ice, land, and land ice. The surface characteristics, as well as turbulent and radiative fluxes, are calculated separately for each kind of surface, while the atmosphere above is assumed to be well-mixed zonally. The atmospheric model uses a realistic land/ocean ratio for each latitude band. More detailed description of the model can be found in Sokolov and Stone (1998) and Prinn et al. (1999).

b. Ocean component

The ocean component of the coupled model is the modular ocean model (MOM2; Pacanowski 1996) with idealized geometry (Fig. 1). It consists of two rectangular "pool" basins connected by a Drake Passage that extends from 64° to 52°S. The Indo-Pacific (hereinafter Pacific) pool extends from 48°S to 60°N and is 120° wide while the Atlantic pool extends from 48°S to 72°N and is 60° wide.

The meridional resolution is 4° and the zonal resolution varies from 1° near the boundaries to 3.75° in the interior of the ocean. Better resolution of the boundary currents has been shown to improve the meridional heat transport in an ocean GCM (Kamenkovich et al. 2000). In the vertical, the model has 15 layers of increasing thickness from 53 m at the surface to 547 m at depth. The bottom of the ocean is flat and 4500 m deep everywhere except in the Drake Passage where there is a sill 2900 m deep. As our Drake Passage extends all the way to Antarctica, the absence of a zonal mean gradi-

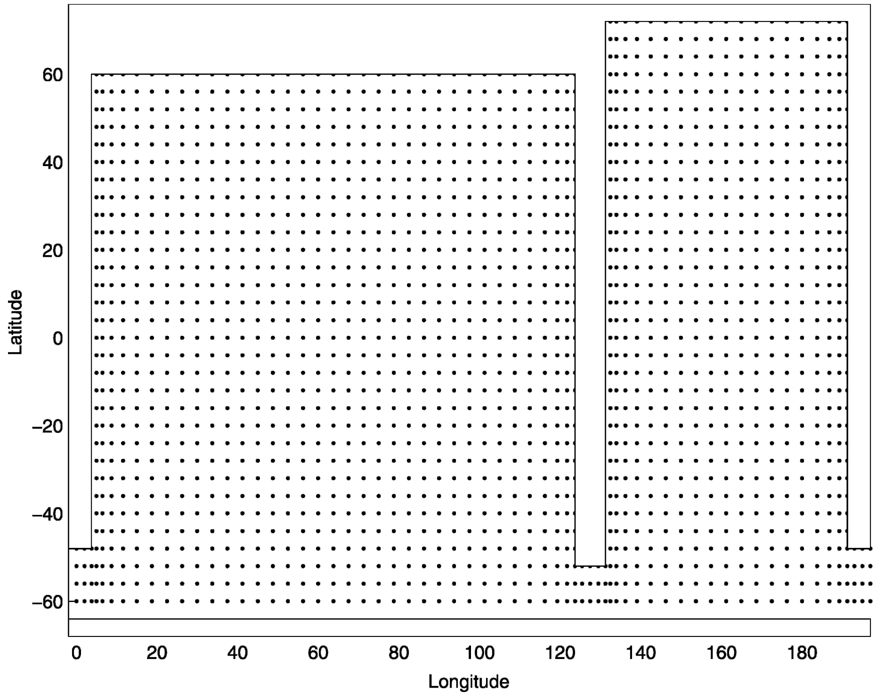

FIG. 1. Geometry of the ocean model and velocity points in the Arakawa B grid.

ent may lead to reduced Antarctic Bottom Water formation in the Southern Ocean (Hughes and Weaver 1994).

No-slip boundary conditions are applied to the lateral walls and free-slip boundary conditions at the bottom of the ocean, except in the Antarctic Circumpolar Current (ACC) where bottom drag is applied so as to obtain a more realistic speed for the ACC. Boundary conditions for tracers are insulating at lateral walls and bottom of the ocean. Since the model does not include any high-latitude basins, no high latitude filter has been employed.

Effects of mesoscale eddies on oceanic stratification are parameterized in this model. The mixing tensor is oriented along isopycnal surfaces (Redi 1982), which limits diapycnal mixing by the mesoscale eddies. The Gent–McWilliams scheme (Gent and McWilliams 1990) is also used. This scheme introduces eddy-induced transport velocities whose main effect is to homogenize isopycnal thickness with strong tendencies to flatten isopycnal surfaces and to effectively reduce the available potential energy. It is noteworthy that since the western boundary current is sufficiently resolved in our coarse-resolution model, the magnitude of spurious numerical diffusion is small (Griffies et al. 2000). No background horizontal diffusivity is used in this model. Table 1 summarizes the mixing parameters of the ocean model in its standard configuration.

c. Coupling, spinup, and experimental setup

The boundary condition for the uncoupled 2D atmospheric model is given by the observed SST from Levitus and Boyer (1994) and sea ice. The uncoupled ocean model is forced by heat and freshwater fluxes and wind stress taken from Jiang et al. (1999). The heat flux boundary condition consists of two terms:

$$H_f = H_{\mathrm{obs}} + C\rho\left(\frac{\mathrm{SST}_{\mathrm{obs}} - \mathrm{SST}}{\lambda}\right)d_1. \tag{1}$$

The first term is the observed heat flux while the second is a relaxation term to the observed SST. The relaxation time (λ) is 60 days and the thickness of the first ocean layer (d_1) is 53 m, C is the specific heat capacity, and ρ is the density of the water. Note that the long-term average of the relaxation term would be zero if the model reproduced the observed sea surface tempera-

TABLE 1. Subgrid-scale parameters of the ocean model in standard configuration.

Parameter	Value	Units
Isopycnal diffusivity	1000	$m^2\ s^{-1}$
Diapycnal diffusivity	0.5	$cm^2\ s^{-1}$
Thickness diffusivity	1000	$m^2\ s^{-1}$
Lateral viscosity	50 000	$m^2\ s^{-1}$
Vertical viscosity	100	$cm^2\ s^{-1}$

ture when forced by the observed heat flux. The freshwater boundary condition for the ocean model is based on precipitation minus evaporation data, river runoff data, and ice-calving data. No salinity restoration is applied to the ocean surface. See Kamenkovich et al. (2002) for a more detail description of the model components spinup.

In the uncoupled spinup, the ocean model is considered having reached equilibrium when the global average heat flux entering the ocean approaches the zero value. This led to integrations of 12000, 6000, 3000, and 1000 yr for diapycnal diffusivity 0.1, 0.2, 0.5, and 1.0 $cm^2 s^{-1}$, respectively. Subsequently the atmospheric and oceanic components are coupled in the anomaly coupling mode described below and they are spun up for an additional 1000 yr for each value of the diapycnal diffusivity.

Coupling takes place twice a day. The atmospheric model calculates 12-h mean values of heat and freshwater fluxes over the open ocean (Ha, Fa), their derivatives with respect to the SST (dHa/dSST, dFa/dSST), and the wind stress. These quantities are then used to calculate the longitudinal variations of the heat and freshwater fluxes for the ocean model in the following way:

$$\mathrm{Hao}(x, y) = \mathrm{Ha}(y) + \left(\frac{d\mathrm{Ha}}{d\mathrm{SST}}\right)(y)[\mathrm{SST}(x, y) - \mathrm{SST}(y)^*], \tag{2}$$

$$\mathrm{Fao}(x, y) = \mathrm{Fa}(y) + \left(\frac{d\mathrm{Fa}}{d\mathrm{SST}}\right)(y)[\mathrm{SST}(x, y) - \mathrm{SST}(y)^*]. \tag{3}$$

SST* denotes the zonal average SST and thus the last terms on the right-hand side allow for the zonal variations of the fluxes as well as the zonal transfer of heat and moisture among ocean basins. The last term in Eq. (3) represents variations in evaporation only—that is, there are no longitudinal variations in precipitation in our model (see Kamenkovich et al. 2002 for more details). The wind stress is independent of longitude. The atmosphere and ocean models are coupled through their anomalous fluxes of heat and freshwater. From Eqs. (2) and (3) the fluxes of heat (Ho) and freshwater (Fo) are

$$\mathrm{Ho}(x, y) = \mathrm{Ho}^{\mathrm{spin}}(x, y) + \mathrm{Hao}(x, y) - \mathrm{Ha}^{\mathrm{spin}}(y), \tag{4}$$

$$\mathrm{Fo}(x, y) = \mathrm{Fo}^{\mathrm{spin}}(x, y) + \mathrm{Fao}(x, y) - \mathrm{Fa}^{\mathrm{spin}}(y), \tag{5}$$

where $\mathrm{Ho}^{\mathrm{spin}}$ and $\mathrm{Fo}^{\mathrm{spin}}$ are the fluxes diagnosed after the spinup of the ocean-only model, and $\mathrm{Ha}^{\mathrm{spin}}$ and $\mathrm{Fa}^{\mathrm{spin}}$ are the fluxes calculated from spinup of the atmospheric model alone. A similar procedure is used for the wind stress. Note that the flux correction is calculated separately for each equilibrium run performed with different diapycnal diffusion and it is fixed for all coupled runs.

The ocean is integrated for 12 h forced by the above fluxes and provides to the atmosphere the zonal mean SST. Asynchronous integration (Bryan 1984) is used, with a 12-h time step for the tracer equations and a 1-h time-step for the momentum equations. This is sufficient to resolve the annual cycle (Kamenkovich et al. 2002). The coupled model takes about 4 h to complete a hundred years integration in a 2.2-GHz Dell workstation with 2-GB memory. For more details about the coupling procedure refer to Kamenkovich et al. (2002).

Peak-to-peak fluctuations of SAT are confined to two tenths of a degree and represent the natural variability of the climate as simulated by this model, comparable with that found in more sophisticated GCMs (Houghton et al. 2001, their Fig. 12.1). The natural variability (estimated by the peak-to-peak variations) of the THC goes from few tenths of Sverdrups (1 Sv ≡ 10^6 $m^3 s^{-1}$) for small diapycnal diffusivity, up to 2 Sv for large diapycnal diffusivity, while in full 3D coupled GCMs the same quantity is of the order of 2–4 Sv (Houghton et al. 2001, their Fig. 9.21).

The Massachusetts Institute of Technology (MIT) earth model of intermediate complexity (EMIC), as other EMICs, is designed to contain the main feedbacks needed to reproduce the behavior of global quantities in more complex GCM while being computationally efficient and suitable for sensitivity experiments as the one in the present study (see Claussen et al. 2002 for a comparison of various EMICs). The uniqueness of the MIT EMIC lies in its configuration: it is the only EMIC we are aware of that couples a 2D statistical-dynamical atmosphere to a 3D ocean GCM.

3. Scaling behavior of the ocean circulation

a. *Thermohaline circulation*

As vertical diffusivity k_υ increases, the thermocline deepens and the THC strength increases, as shown in Fig. 2 for the Atlantic Ocean. In the mid- and high-latitude North Pacific, there is little change in meridional overturning, as there is only weak circulation in this region in either the large or small k_υ runs (Fig. 3). However, as shown in this latter figure, there is considerable increase in upwelling in the tropical and subtropical Pacific for larger k_υ.

Using idealized geometry, single-hemisphere (rapidly restored) ocean models, it has been shown robustly that the scaling of overturning follows an approximate

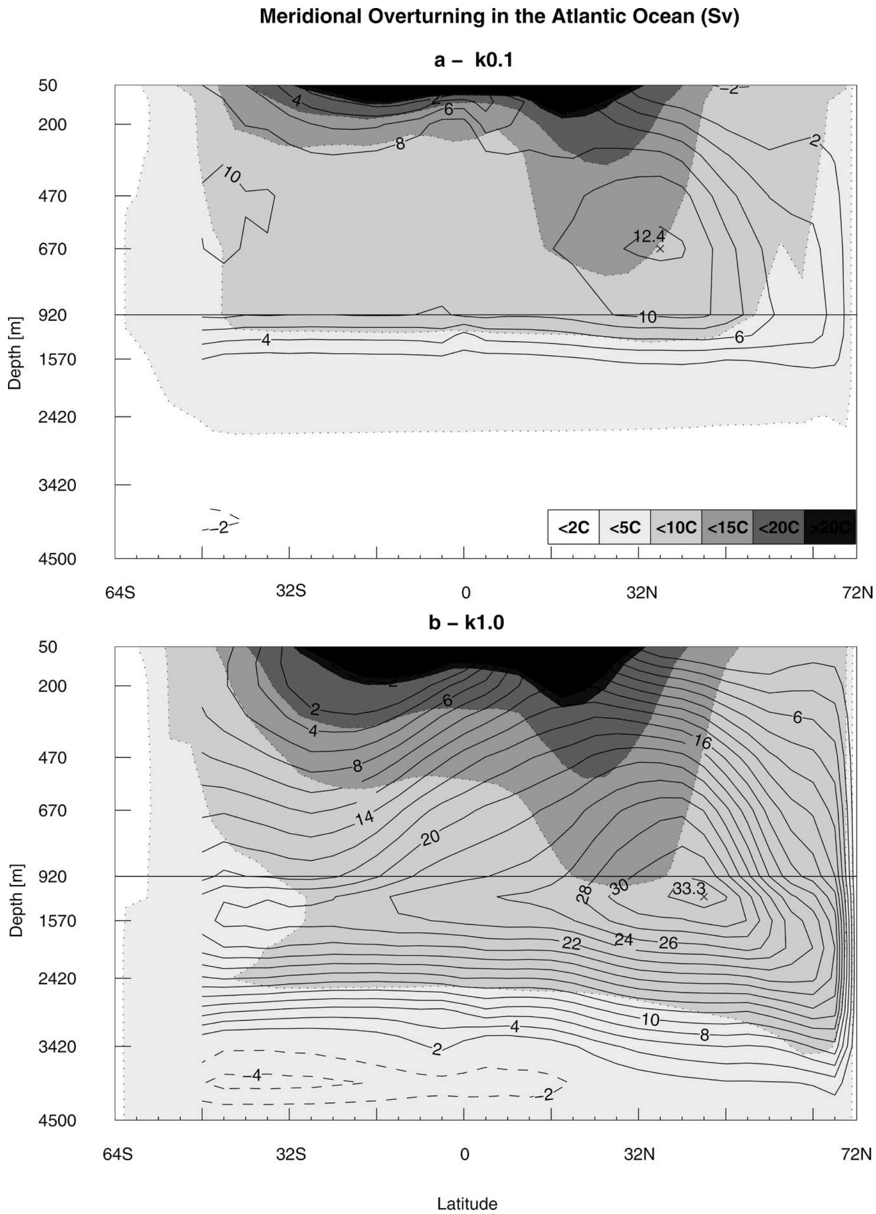

FIG. 2. Meridional streamfunction of the Atlantic Ocean at equilibrium for diapycnal diffusivity (a) 0.1 and (b) 1.0 $cm^2 s^{-1}$. Solid line for clockwise overturning and dashed line for anticlockwise overturning. Shading indicates temperature according to the scale in (a).

two-thirds power law (Bryan 1987; Colin de Verdiere 1988; Park and Bryan 2000; Scott 2000). This power law is supported by a simple scaling relationship (Welander 1971) and a more complicated theory for the overturning circulation (Marotzke 1997), both of which are grounded in the thermal wind relationship. Here, our coupled model is considerably more complex: we have a more complicated "boundary condition" at the ocean surface because of the coupling, we include wind forcing and we have a global configuration (i.e., a multibasin interhemispheric circulation connected by a circumpolar channel). Nevertheless, we present a scaling analysis in the spirit of the canonical single-hemisphere results, as shown in Fig. 4 for the North Atlantic maximum and Fig. 5 for the South Pacific maximum (observed roughly at 32°S).

In both cases, an approximate straight-line fit is observed. In the North Atlantic, the overturning maximum scales as the 0.44 power (as measured by a best-fit line), whereas in the South Pacific the maximum scales

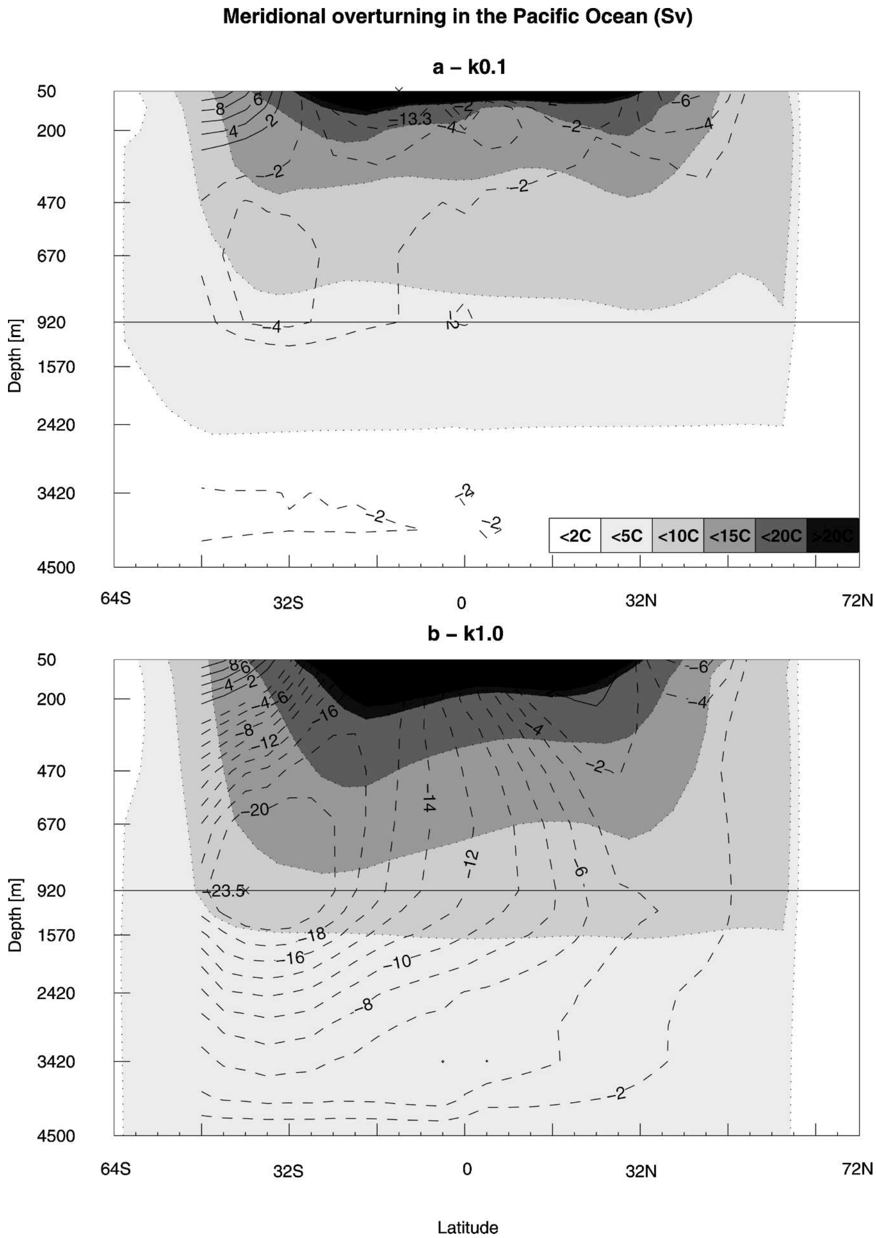

FIG. 3. Same as Fig. 2 but for the Pacific Ocean.

as the 0.63 power. We are aware of only two studies which examine the scaling of meridional overturning in a global model, Wright and Stocker (1992) and Knutti et al. (2000), both using a simplified ocean model consisting of interconnected zonally averaged ocean basins. Wright and Stocker's results (best-fit scaling laws of 0.46 and 0.68 for the Atlantic and Pacific, respectively) are close to ours, despite their use of relaxation boundary conditions for temperature and salinity. Knutti et al. (2000) obtains roughly the same result for the North Atlantic maximum, again using restoring boundary conditions. This later study uses the Gent–McWilliams parameterization for mesoscale eddies, as does our model.

We now address the differences between our model and those used in past studies, and how these differences might affect the observed scaling behavior.

1) (LOCAL) WIND FORCING

Local wind forcing does affect the depth of the zonally averaged thermocline, which presumably has some effect on the meridional overturning circulation (by lo-

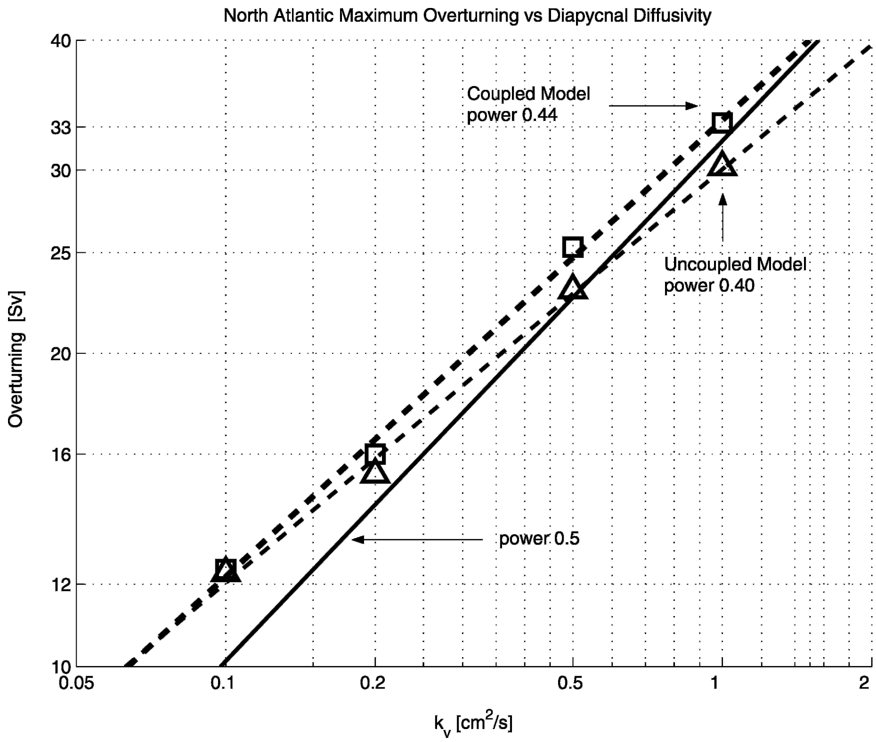

FIG. 4. Maximum in the meridional streamfunction of the North Atlantic Ocean for coupled (squares) and uncoupled (triangles) model at equilibrium vs diapycnal diffusivity (k_v). Log–log plot. Linear regression lines are dashed while the solid line shows the relation $(k_v)^{0.5}$ for comparison.

cal, we mean intrahemispheric wind forcing; we will address wind forcing over the southern channel below). However, past studies that examine the single-hemisphere scaling with and without wind forcing suggest only a modest wind effect (Zhang et al. 1999; Vallis 2000), most noticeable at low diffusivities (i.e., the overturning does not drop off as dramatically if wind forcing is present). Thus, local winds might boost the maximum overturning slightly for our weak kappa runs, particularly our 0.1 and 0.2 cm^2 s^{-1} experiments, but we would not expect it to preclude us from obtaining a scaling relationship similar to that of the simple models.

2) Atmospheric coupling

In the canonical model results, temperature (and/or density) is either prescribed or rapidly restored at the surface. Here, we have a flux condition for freshwater forcing. Our effective boundary condition for temperature (i.e., from the coupled atmosphere) is a hybrid flux-relaxation boundary condition: although the loss of heat at the ocean surface is closer in spirit to a flux boundary condition, we do use a "flux adjustment" and thus our runs effectively include a relaxation component. We also show the scaling of maximum overturning in the North Atlantic with k_v for the uncoupled model; not surprisingly, there is only a slight change in the best-fit power law.

Thus, we conclude that the most significant novelty with respect to the surface boundary conditions is our use of a freshwater flux (note this flux is little changed between the different k_v runs). Zhang (1998) and Zhang et al. (1999) are the only studies that we are aware of that examine the scaling argument given mixed boundary conditions, albeit in an idealized single-hemisphere configuration. Using salinity conservation in a single hemisphere, these authors show that when haline forcing dominates, a 1/2 power law emerges, whereas a 2/3 law is recovered for dominant temperature forcing. Zhang (1998) found an approximate 1/2 power law for flux conditions in temperature and salinity, but did not show a comparable scaling for mixed boundary conditions. Although it is not clear to what extent, if any, the analytical scaling of Zhang et al. (1999) applies to our configuration, it is interesting that we too achieve an approximate 1/2 power law in the North Atlantic, where salinity forcing is thought to play a large role in determining the rate of sinking. In the South Pacific, however, our observed scaling law is

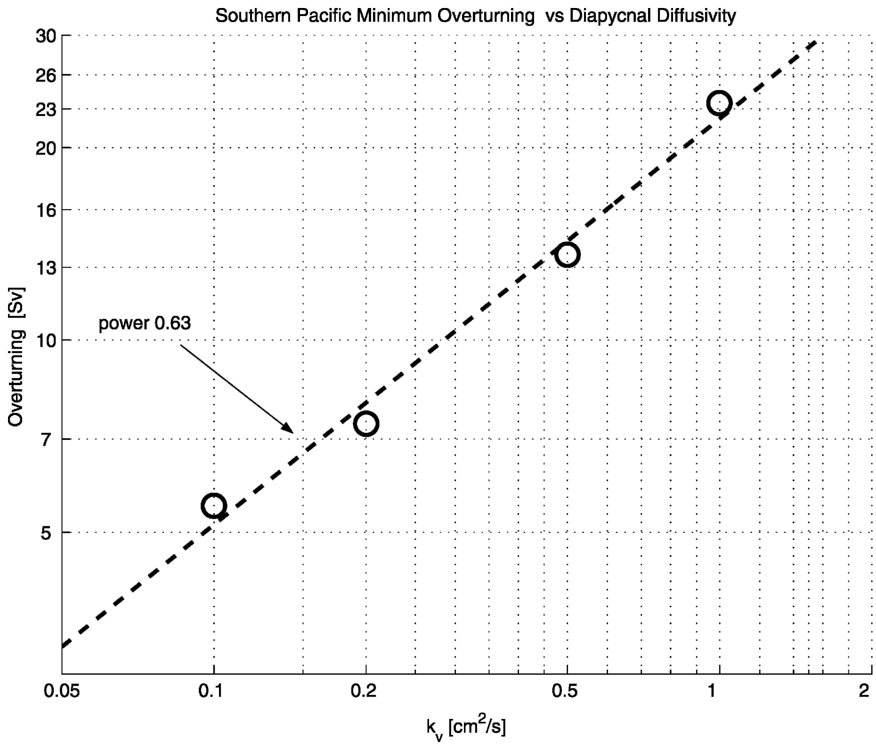

FIG. 5. Minimum in the meridional streamfunction of the South Pacific Ocean (circles) at equilibrium vs diapycnal diffusivity (k_v). Log–log plot. Linear regression line is dashed.

closer to that predicted by Zhang's temperature-dominated extreme.

3) GLOBAL CONFIGURATION

While the role of mixing is straightforward in the idealized single-hemisphere configuration, there is considerable debate as to the importance of mixing in the global configuration. Specifically, Toggweiler and Samuels (1995) argue that wind forcing over the ACC effectively controls the rate of sinking in the North Atlantic. Gnanadesikan (1999) presents a simple theory for overturning in a single-ocean basin with a circumpolar channel, effectively combining the effect of wind forcing (in the channel) and diapycnal mixing; the scaling here has been verified in other models studies (Klinger et al. 2003). Unfortunately, Gnanadesikan's model produces a cubic equation governing pycnocline depth, and therefore would not predict a simple power-law scaling. Moreover, in this theory, all mixing-induced upwelling occurs in the Tropics of the single basin, whereas our model is a multibasin configuration. In fact, it seems reasonable to assume that most of the mixing-induced upwelling occurs in the Pacific Basin, given the greater area. The work of Bugnion et al. (2004b) supports this idea: the adjoint sensitivity of the THC strength to the diapycnal diffusion is large in the tropical regions of all ocean basins.

Hence, we argue that although the sinking in the Northern Atlantic is the traditional focus of climate research, the scaling of the South Pacific cell is the closer comparison to the canonical single-hemisphere studies. This conjecture is supported by the near agreement of our power-law fit with the classical 2/3 power law (Fig. 5). The scaling of the North Atlantic is more problematic. It is not clear what the y intercept in Fig. 4 should be, but it does seem to imply a significant residual Circulation in the "no-mixing" limit. Further exploration of THC scaling in a global configuration is left for future studies.

b. Heat transport

In the Northern Hemisphere, the power-dependence between global ocean heat transport and diapycnal diffusivity is 0.24 (Fig. 6). At the location of the maximum transport (from 18°N for diffusivity 0.1 cm^2 s^{-1} to 26°N for diffusivity 1.0 cm^2 s^{-1}), the strength of the meridional streamfunction for the global ocean depends on the 0.37 power of the diapycnal diffusivity (Table 2). At the same location, the temperature difference between the poleward and equatorward branches of the North

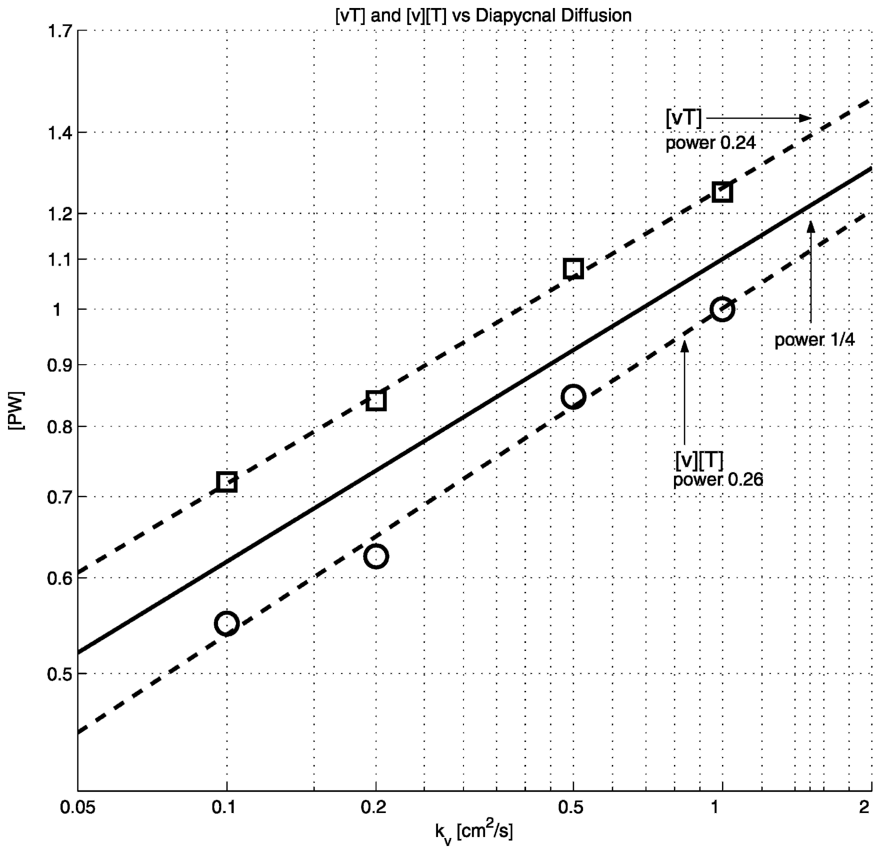

FIG. 6. Maximum poleward heat transport [(vT), squares] and heat transport by the mean meridional circulation [$(v)(T)$, circles] for the global ocean at equilibrium vs diapycnal diffusivity (k_v). Log–log plot. Both (v) and (T) are normalized by their value at diffusivity 1.0 cm^2 s^{-1}. Linear regression lines are dashed while the solid line represents the relation $(k_v)^{0.25}$.

Atlantic overturning cell goes from 26°C, for diffusivity 0.1 cm^2 s^{-1}, to 20°C, for diffusivity 1.0 cm^2 s^{-1}, having a -0.12 power dependence on the diapycnal diffusivity (Table 2). The product of overturning strength and the temperature difference between the poleward and equatorward branches of the North Atlantic overturning cell explains the relation between the maximum heat transport and the diapycnal diffusivity (Fig. 6). In our model, in fact, the main component of the poleward heat transport is given by the thermohaline circulation. Both in spinup and coupling procedure the SST is restored to its zonal average [Eqs. (1) and (2)], hence the heat transport by the gyre circulation is greatly reduced. The absence of heat transport by the gyre circulation explains why the North Pacific contribution to the global heat transport in the Northern Hemisphere is negligible (Fig. 7c). A recent estimate for the heat transport in the real ocean (Ganachaud and Wunsch 2003) is as follows: 1.2 PW at 20°N and 0.8 PW at 20°S in the Atlantic Ocean; 0.5 PW at 20°N and -1.5 PW at 20°S in the Indo-Pacific Ocean. Our high-diffusivity runs have values comparable to the real world estimates in the North Atlantic and South Pacific where the heat transport by the overturning circulation domi-

TABLE 2. Sensitivity of heat transport to the diapycnal diffusivity: (A) maximum heat transport, (B) maximum streamfunction, and (C) temperature difference between the poleward and equatorward branches of the North Atlantic overturning cell. Both B and C are calculated at the location of maximum global ocean heat transport.

	Diapycnal diffusivity	cm^2 s^{-1}	0.1	0.2	0.5	1.0
A	Maximum heat transport	PW	0.72	0.84	1.08	1.25
B	Maximum streamfunction at A	Sv	11.4	12.8	19.8	26.0
C	THC vertical temperature difference at A	°C	26.2	25.1	22.1	20.3

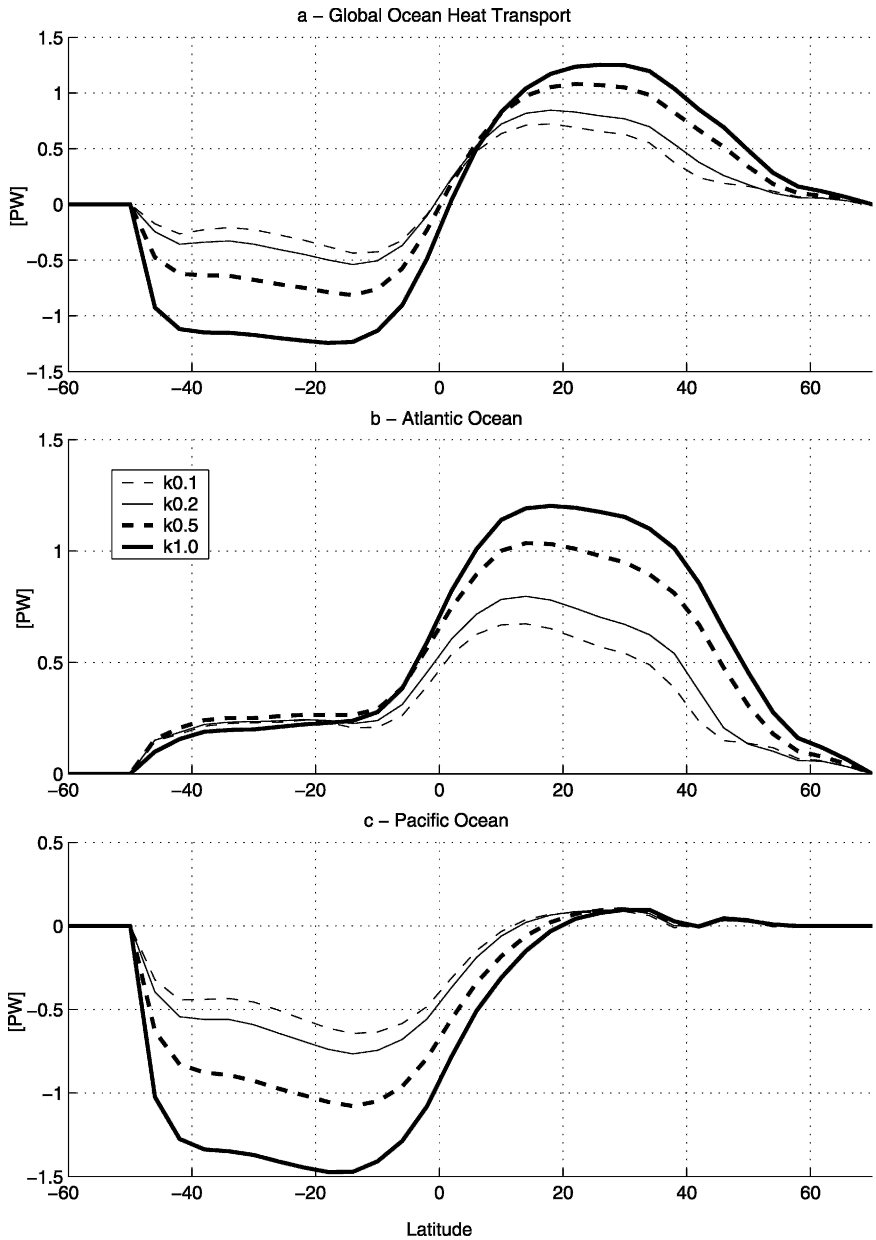

FIG. 7. Poleward heat transport for the (top) global ocean, (middle) Atlantic Ocean, and (bottom) Pacific Ocean for diapycnal diffusivity 0.1 $cm^2 s^{-1}$ (thin dashed line), 0.2 $cm^2 s^{-1}$ (thin solid line), 0.5 $cm^2 s^{-1}$ (thick dashed line), and 1.0 $cm^2 s^{-1}$ (thick solid line).

nates. The difference between the model values and the real-world estimates are most noticeable in the South Atlantic and in the North Pacific where the gyre circulation transports a considerable amount of heat poleward. The scaling law of the heat transport will differ if the gyre transport contribution from the North Pacific Ocean is included.

In the Southern Hemisphere, the dependence of the poleward heat transport to the diapycnal diffusion goes with the power of 0.45 for the global ocean and 0.35 for the Pacific component (not shown). Although the Pacific Ocean contributes the most to the global heat transport in the Southern Hemisphere, the Southern Atlantic contribution cannot be ignored (Figs. 7b,c). The latter is relatively insensitive to the diapycnal diffusivity explaining the decrease of power from the global ocean heat transport to the Pacific component in the Southern Hemisphere. The insensitivity of the Southern Atlantic heat transport to diapycnal diffusion may be relevant for the behavior of the THC. The strength of the THC is correlated with the steric height difference between the Northern and Southern Atlantic (Hughes and Weaver 1994; Thorpe et al. 2001), which in turn is related to the integrated density over a water column. At each latitude band, the heat transport, or better its divergence, affects the density of the water column thus the THC strength. This version of the MIT EMIC has idealized geometry; in particular the African continent extends to 48°S rather than a more realistic 30°S. Moreover, processes like brine rejection, responsible for the formation of the Antarctic Bottom Water, are not modeled. Hence the insensitivity of the Southern Atlantic heat transport to the diapycnal diffusivity may be biased in our model. Further investigation with a realistic geometry coupled GCM is needed.

In general we find a smaller power-law dependence between oceanic heat transport and diapycnal diffusivity compared to previous studies with OGCMs, as one would expect for a coupled model. Our findings do not agree with the scaling argument either in the Northern Hemisphere or in the Southern Hemisphere. The scaling argument may need to be revised to include feedbacks between the ocean and the atmosphere and the effect of realistic Southern Ocean geometry. In addition, as seen above, the temperature difference between the poleward and equatorward branches of the North Atlantic overturning cell affects the power-law for the Northern Hemisphere heat transport. The temperature difference sensibly depends on the temperature of the water sinking in the North Atlantic, which depends, among other things, on the ocean overturning circulation and both the atmospheric and oceanic meridional heat transports. The scaling argument, by its construction, cannot capture the relation between the above-mentioned temperature difference, the strength of the overturning, and the meridional heat transports.

4. Vertical heat balance

a. Control experiment

The vertical heat balance of the global ocean consists of downward diapycnal diffusion and Eulerian advection (hereinafter advection) balancing upward fluxes by isopycnal diffusion and bolus velocity (hereinafter GM) advection (Fig. 8a). Convection plays a negligible role in all runs, the reason being explained in the appendix. Following Gregory (2000), we divide the global ocean in three latitude bands: the Southern Ocean, southward of 30°S, the Tropics, between 30°S and 30°N, and the Northern Ocean, northward of 30°N.

Diapycnal diffusion, the major contributor to the downward heat flux for the global ocean (Fig. 8a), is concentrated in the tropical region although considerable diapycnal flux also occurs at high latitudes (Figs. 8b–d). However, while the tropical diapycnal flux is due to the presence of strong vertical temperature gradients, in high latitudes the diapycnal flux arises to partially compensate for the stronger and opposite isopycnal flux (Figs. 8b,d). Eulerian advection takes heat downward at high latitudes but mostly in the Northern Ocean (Figs. 8b,d) and upward in the Tropics (Fig. 8c) so that the global contribution of the advective flux is the smallest among all the components[2] (Fig. 8a). Additionally, GM advection and isopycnal diffusion dominate at high latitudes, where the isopycnal slope is elevated (Figs. 8b,d). The Northern Ocean fluxes are representative of the North Atlantic region, where most of the dynamics in this model takes place, while fluxes in the tropical Pacific are about twice as large as the tropical Atlantic ones (not shown), because the area extent of the former is twice the area of the latter. Note that the convergence of the total meridional heat flux in each basin just balances the divergence of the total vertical flux shown in the figure, as the storage term is negligible.

Figure 8 does not include the surface heat flux, presented in Fig. 9. Heat is entering in the tropical region at a rate of 13 W m^{-2} (16 W m^{-2} Atlantic and 11 W m^{-2} Pacific) and leaving the ocean at high latitudes at a rate of -13 W m^{-2} in the Southern Ocean and -23 W m^{-2} in the Northern Ocean (-53 W m^{-2} Atlantic and -4 W m^{-2} Pacific).

Locally, downwelling occurs in the east side of the North Atlantic basin. The deep water formed in this region flows westward and southward for upwelling in the western side of the basin, as well as in the Southern Ocean and in the interior of the basins (Fig. 10a). Downward advection steepens the isopycnals, which leads to intensified mixing by the eddy-induced velocities of the Gent–McWilliams scheme. Hence, strong Eulerian advective fluxes are contrasted by equally strong and opposite GM fluxes throughout the oceans (Fig. 10b). At high latitudes, diapycnal diffusion tends to compensate isopycnal diffusion (Figs. 10c,d).

Gregory (2000) performed an analysis of the heat balance at 160-m depth for the HadCM2 climate model combining together diffusive fluxes (isopycnal and diapycnal) while the advective fluxes are Eulerian only since no GM scheme is employed. The author finds that, for the global ocean, total downward heat advection is balanced by upward diffusion, opposite to the balance assumed in one-dimensional upwelling-diffusion models. In HadCM2, Southern Ocean fluxes

[2] This is excluding convection.

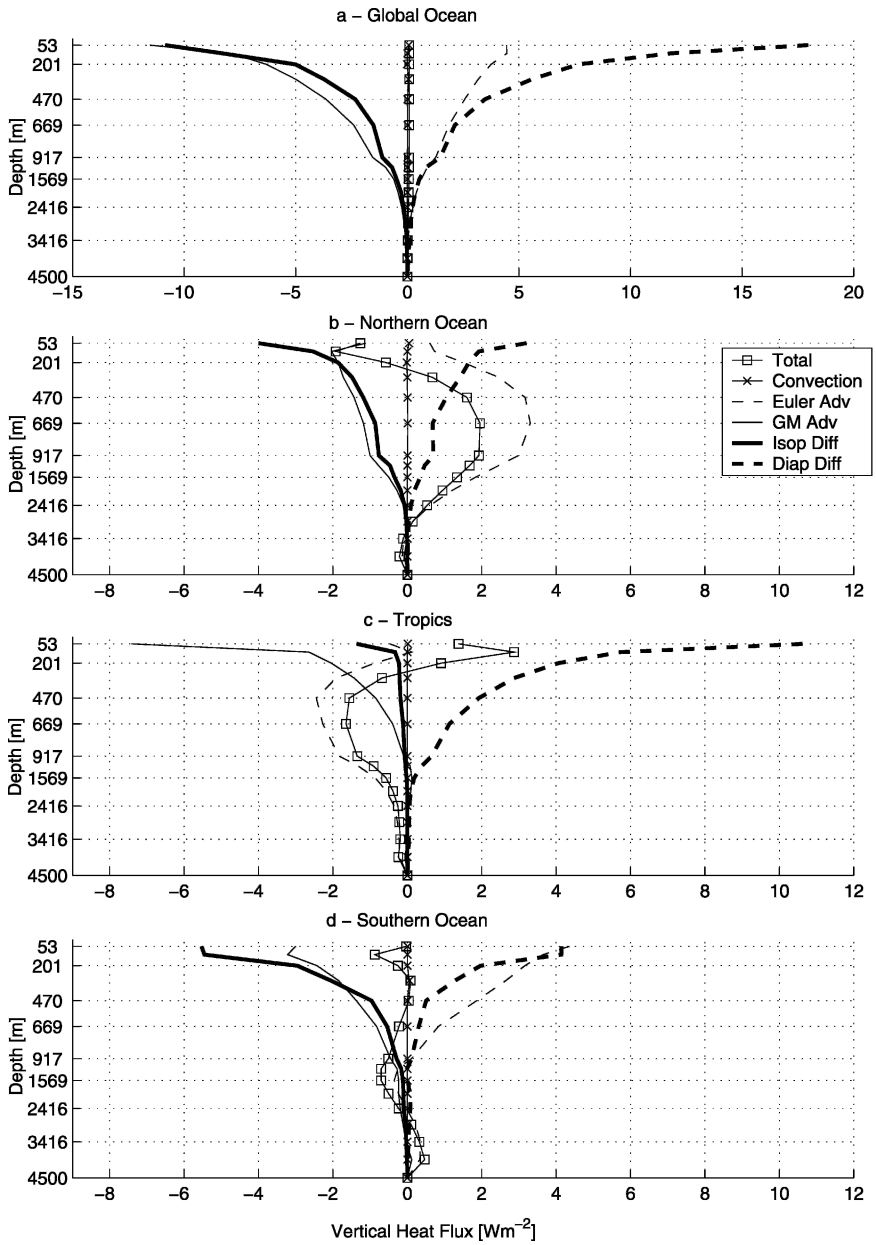

FIG. 8. Vertical heat flux components for (a) global ocean, (b) Northern Ocean, (c) Tropics, and (d) Southern Ocean for diapycnal diffusivity 0.5 cm^2 s^{-1}. Positive (negative) sign for downward (upward) fluxes. Note the change of scale in (a).

dominate the global budget, thanks to a strong Deacon cell (47 Sv) that extends from 35° to 65°S. Heat is taken down at 35°S by advection and it is lost along the way by isopycnal diffusion. Water then upwells in much colder sites around 65°S. In the MIT EMIC the Deacon cell is significantly weaker (18 Sv) and its extension is limited between 48° and 64°S. Although the vertical heat balance at different latitude bands in our model agrees with Gregory's (2000) picture (downward advection balances upward diffusion at high latitudes and the opposite in the Tropics), the global budget for the MIT EMIC in its standard configuration is dominated by the tropical region, thus opposite to Gregory (2000) and in agreement with one-dimensional upwelling-diffusive models. However, for lower diffusivity values and below 1000 m, also the MIT EMIC presents a global heat balance in accordance with Gregory (2000) as will be illustrated in the next section.

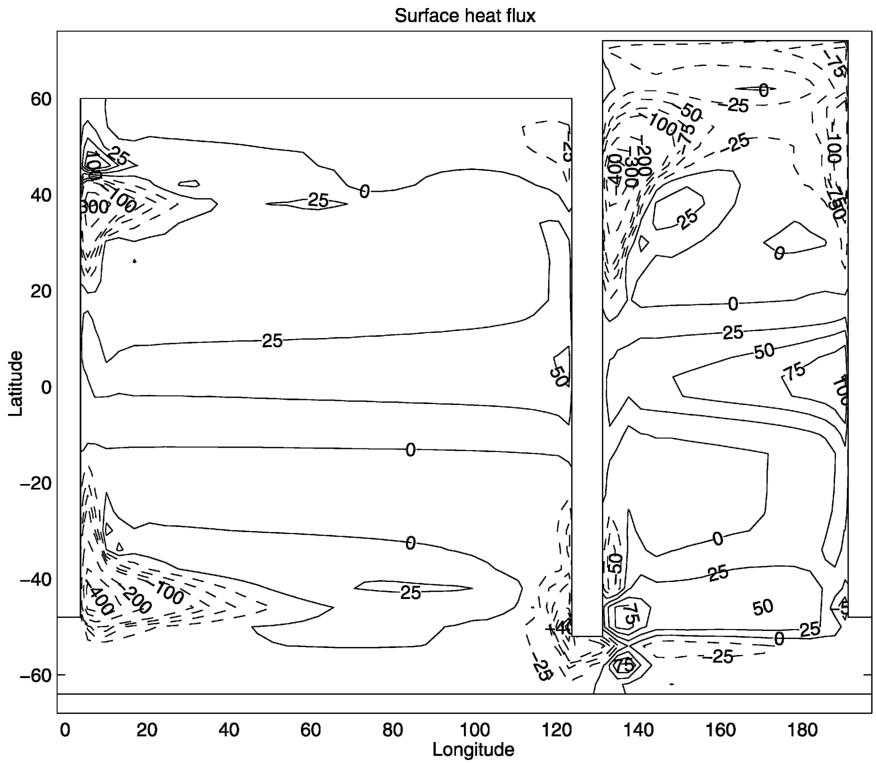

FIG. 9. Surface heat flux in W m^{-2} for diapycnal diffusivity 0.5 cm^2 s^{-1}. Contour interval is 25 W m^{-2} between -100 and 100 W m^{-2}, and it is 100 W m^{-2} outside this range. Solid (dashed) line for positive (negative) values.

b. Sensitivity to diapycnal diffusion

Four control experiments have been carried out, with the same model being spun up with different values of the diapycnal diffusivity, namely: 0.1, 0.2, 0.5, and 1.0 cm^2 s^{-1}. Although the current estimates for the global average diapycnal diffusivity are 0.2 (Huang 1999) and 1.0 cm^2 s^{-1} (Munk and Wunsch 1998), we compare in detail the differences between the control runs with diapycnal diffusivity 0.1 and 0.5 cm^2 s^{-1}, referring to the former case as the "small diffusivity model" and to the latter as the "standard diffusivity model." The conclusions drawn for the small diffusivity model can be applied to the simulations using diapycnal diffusivity 0.2 cm^2 s^{-1} while the standard diffusivity case is similar, in its behavior, to the simulation with diapycnal diffusivity 1.0 cm^2 s^{-1}. The reason behind the choice for diapycnal diffusivity 0.1–0.5 cm^2 s^{-1} instead of 0.2–1.0 cm^2 s^{-1} is that the former doublet gives a more representative range of where the strength of the THC in the real ocean may be found. The strength of the THC for the experiments with diapycnal diffusivity 0.1 and 0.5 cm^2 s^{-1} is 12 and 26 Sv, respectively, while the latest estimates for the same quantity is 15 Sv (Ganachaud and Wunsch 2003).

In the experiments with small diffusivity, there remains a very small net flux into the ocean, even after very long integration times (12 000 yr in the case of diffusivity 0.1). Nevertheless the qualitative result is clear. The vertical heat balance for the small diffusivity model is not much different from the standard diffusivity model. Isopycnal diffusion and GM advection dominate the removal of heat from the deep ocean at high latitudes while advection in the Northern Ocean is a major heat source for the deep ocean. The major difference between the two simulations is in the tropical region. The diapycnal flux is significantly reduced in the small diffusivity model, as expected, and it is no longer the major heat source for the deep ocean, as it is for the standard diffusivity model (not shown). Moreover, the advective flux, upward in the tropical region, is sensibly reduced, hence the total advective flux, downward for the global ocean, slightly increases for the small diffusivity model. In fact, the strength of the THC strongly decreases with decreasing diapycnal diffusivity (Fig. 2) but compensation between decrease in downward warming at high latitudes and decrease in upward cooling in the Tropics leads to a small increase in the global advective flux. As for the standard diffusivity model, in

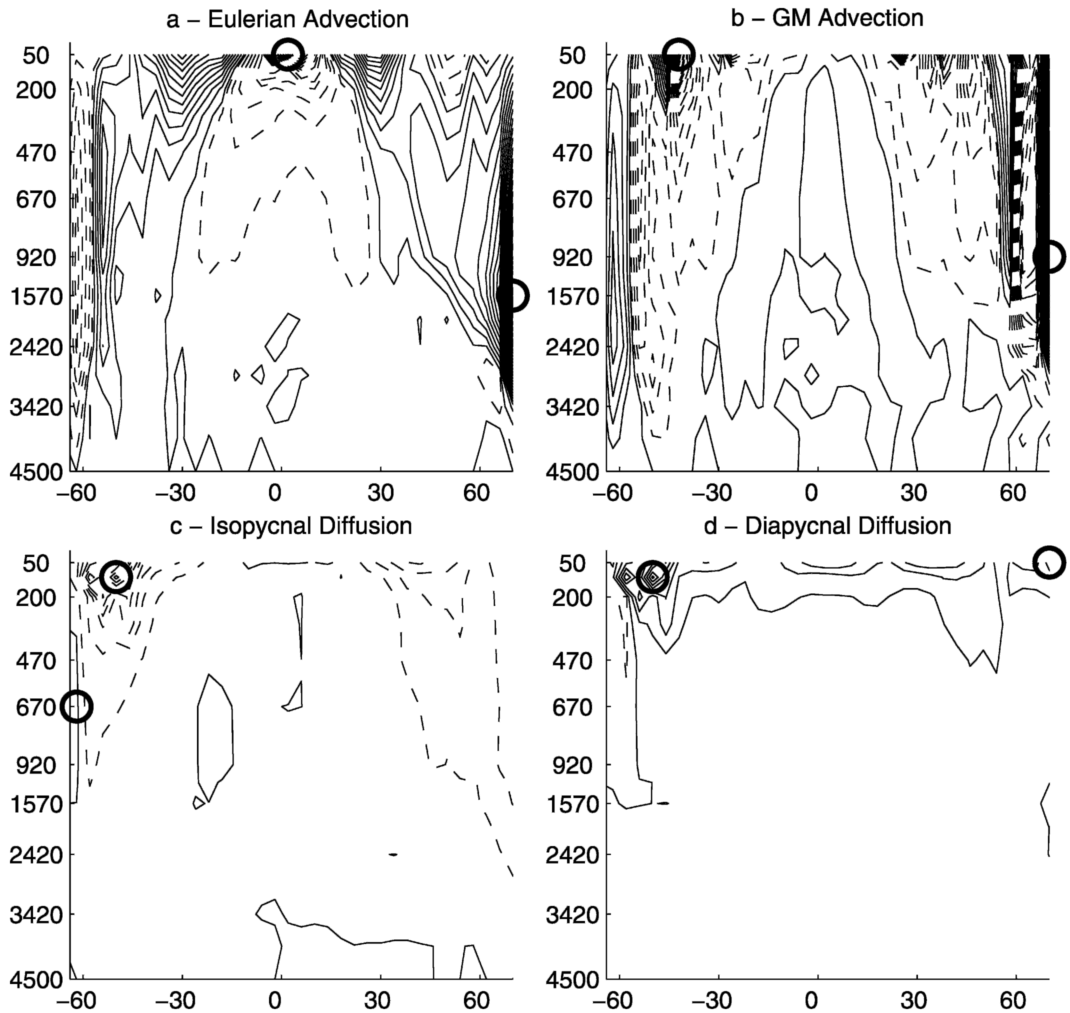

FIG. 10. Zonally averaged vertical heat flux components for global ocean and diapycnal diffusivity 0.5 $cm^2 s^{-1}$: (a) Eulerian advection, (b) GM advection, (c) isopycnal diffusion, and (d) diapycnal diffusion. Solid (dashed) line for downward (upward) fluxes. Circles denote the position of the maximum and minimum.

the small diffusivity model the tropical region is dominated by the Pacific basin, while the Northern Ocean is dominated by the Atlantic basin.

The magnitude of all fluxes is reduced with smaller diapycnal diffusivity (Fig. 11) as expected from adjoint sensitivity studies (Huang et al. 2003, their Figs. 5 and 11). Total advection always balances total diffusion since convection is always negligible in this version of the MIT EMIC. Fluxes at the bottom of the first layer of the ocean are 0.7 W m^{-2} in the small diffusivity model (Fig. 11a) and one order of magnitude larger for the standard diffusivity model (Fig. 11c), rapidly decreasing with depth. Reduced diapycnal diffusion leads to smaller diapycnal fluxes and shallower thermocline at tropical latitudes. As a consequence, the isopycnal slopes at high latitudes are reduced and so are the vertical isopycnal and GM fluxes. However, in the small diffusivity case, the Tropics are no longer the dominant region at all depths, as it is for the standard diffusivity model, and in the upper 800 m of ocean, the advective–diffusive balance is reversed (Figs. 11a,c).

5. Quasi-static freshwater perturbation

One key question about the equilibrium state of the ocean is whether there is a threshold for the size of perturbations beyond which the circulation changes radically. In particular models generally show such a threshold when the moisture flux into high latitudes of the North Atlantic is increased (Rahmstorf 1995). This behavior can be illustrated by a hysteresis curve, which shows how the equilibrium state of the thermohaline circulation depends on this moisture flux (Rahmstorf 1995). This hysteresis curve has been calculated by the

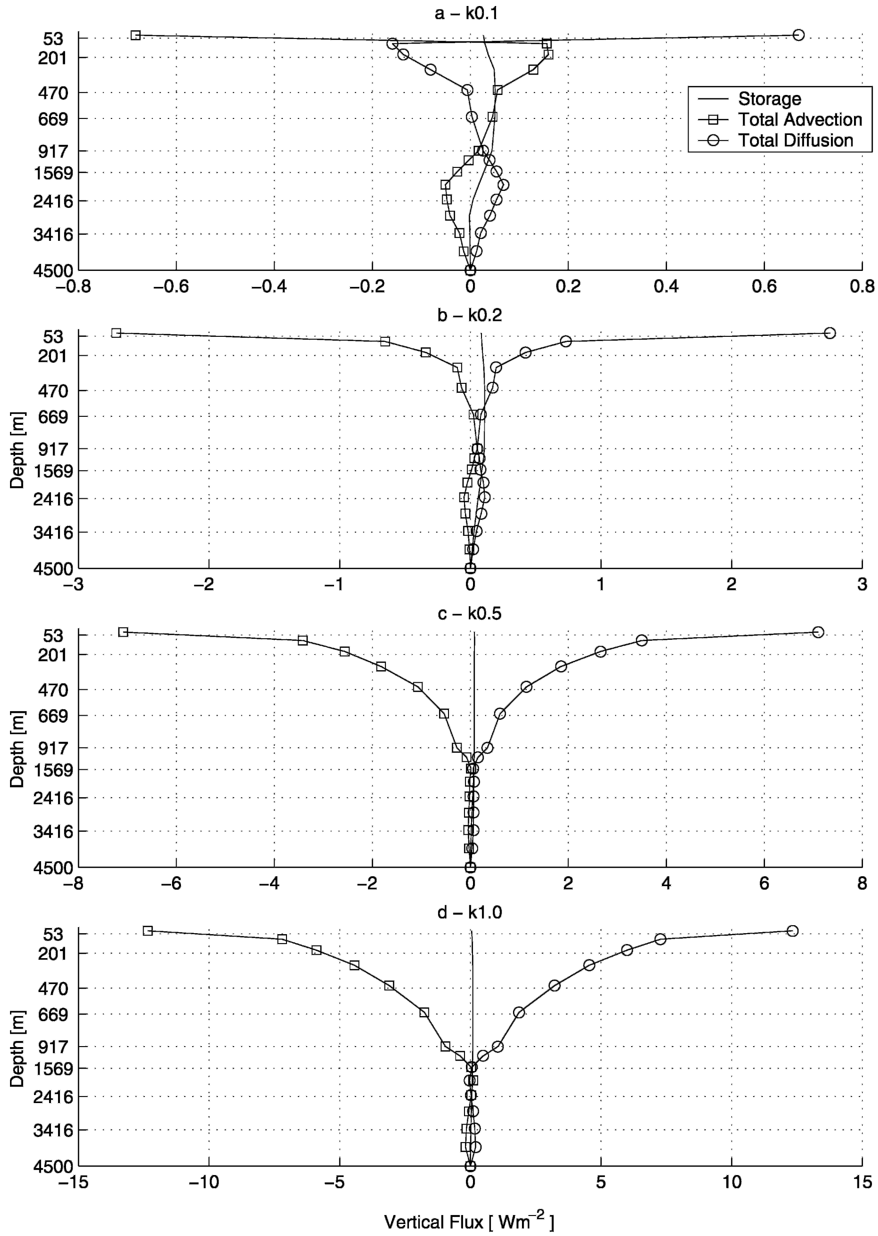

FIG. 11. Heat balance for the global ocean for diapycnal diffusivity (a) 0.1, (b) 0.2, (c) 0.5, and (d) 1.0 cm^2 s^{-1}. Positive (negative) sign for downward (upward) fluxes. Note the change in horizontal scales.

MIT EMIC for two different values of the diapycnal diffusion. The result is depicted in Fig. 12. Note that, in the hysteresis experiments, the freshwater input is not balanced by any freshwater export in other regions of the oceans, therefore the global salinity is not conserved. As in previous sensitivity studies of the hysteresis curve (Ganopolsky et al. 2001; Schmittner and Weaver 2001; Prange et al. 2003), the circulation is more unstable for a smaller value of the diapycnal diffusivity. To induce the THC to collapse, a freshwater input of 0.52 Sv is needed with diapycnal diffusivity of 0.5 cm^2 s^{-1} while 0.37 Sv are needed with 0.2 cm^2 s^{-1} diapycnal diffusivity. The main reason for the early collapse in low vertical diffusion models is most likely related to their smaller overturning in the equilibrium state. The equilibrium overturning strength for the current climate is proportional to the diapycnal diffusivity (Bryan 1987) therefore also the salt transport into high latitudes. The latter helps sustain the thermohaline circulation, hence the system is more unstable to freshwa-

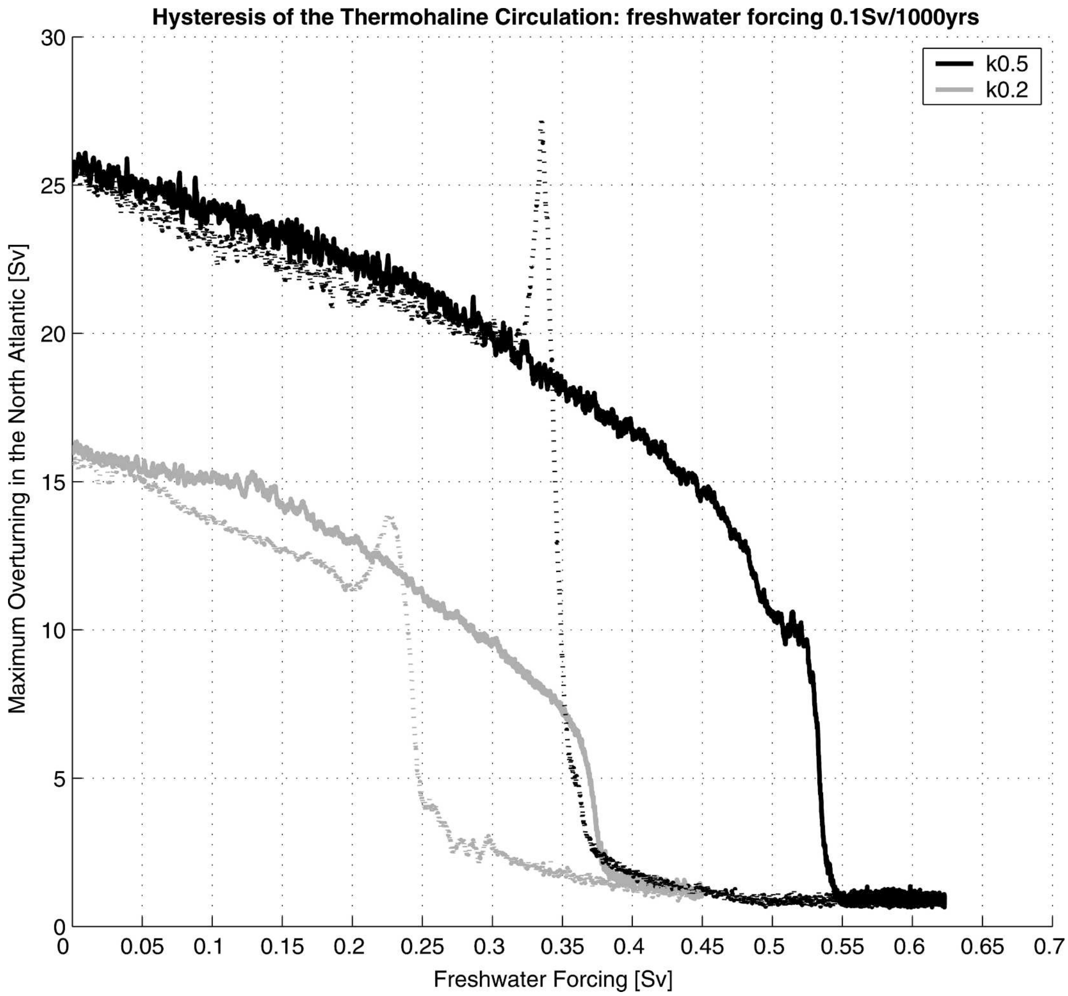

FIG. 12. Hysteresis cycle of the THC for diapycnal diffusivity 0.5 and 0.2 $cm^2 s^{-1}$. The additional moisture flux was uniformly distributed between 20° and 48°N in the Atlantic basin.

ter perturbations for weaker equilibrium meridional circulation.

The THC collapses around 10 Sv in the standard diffusivity model (0.5 $cm^2 s^{-1}$) and around 6 Sv in the low diffusivity model (0.2 $cm^2 s^{-1}$). Thus, a common threshold for the collapse does not exist in this particular model as in the uncoupled 3D OGCM of Prange et al. (2003). In coupled 2D models with a multibasin ocean component (Ganopolsky et al. 2001; Schmittner and Weaver 2001), threshold for the collapse of the THC is relatively insensitive to the diapycnal diffusivity, suggesting that the oversimplified dynamics of 2D models affects the stability characteristic of the THC.

For smaller values of the diapycnal diffusivity, a smaller amount of freshwater forcing is needed to allow the recovery of the THC. The thermohaline circulation resumes when the freshwater forcing in the North Atlantic is about 0.34 Sv for diapycnal diffusivity 0.5 $cm^2 s^{-1}$ and 0.23 Sv for diapycnal diffusivity 0.2 $cm^2 s^{-1}$. This is in agreement with the behavior of 2D multibasin ocean models but in contrast with the 3D model behavior of Prange et al. (2003). When the THC is in the "shutdown" mode, the previous authors notice that the gyre transport gives an important contribution to the salt balance at the surface in the North Atlantic. Thus, differences in gyre transport can be used to explain the different freshwater threshold for the recovery of the THC. This argument can be employed also to explain the differences between our model and the Prange et al. (2003) model. In the coupling procedure between the 2D atmosphere and the 3D ocean (section 2c), both heat and freshwater fluxes are relaxed toward the global zonal mean as an attempt to capture the zonal variations of the fluxes [Eqs. (2) and (3)]. The consequence is a reduced gyre transport, as confirmed by the small northward heat transport in the North Pacific (Fig. 7c).

The Prange et al. (2003) model employs linear momentum equations and it lacks feedback between the ocean and the atmosphere, two important differences from the MIT EMIC. It is not clear how these differences would affect the hysteresis curve although the former model is clearly sensitive to the formulation of the surface boundary conditions (Prange et al. 2003, their Fig. A4).

For both values of the diapycnal diffusivity, the strength of the THC in the recovery process overshoots the value obtained when increasing freshwater flux. This is indicative of a fast rate of decrease in the forcing. Two additional experiments have been carried out to verify that the THC passes through quasi-steady states when the freshwater flux is increasing. For diapycnal diffusivity 0.2 $cm^2 s^{-1}$, the freshwater flux has been stabilized at 0.2 and 0.3 Sv for 500 yr. In both cases, the THC keeps on slowing down for about 100–150 yr but it partially recovers and stabilizes within 300 yr (not shown). Hence, the model can be considered to be in quasi-steady state for each value of the freshwater forcing. However, for sudden shifts in the regime of the circulation, the departure from equilibrium can be substantial. A slower rate of decrease in the freshwater flux would keep the model closer to equilibrium and avoid overshooting.

The ocean circulation becomes more sensitive to freshwater perturbations as the diapycnal diffusivity decreases—that is, a smaller freshwater perturbation will cause the collapse of the Thermohaline Circulation. To the extent that global warming experiments lead to an increase of freshwater in the North Atlantic (Manabe and Stouffer 1994), the latter statement could be extended to global warming experiments as well. The distance of the equilibrium climate from the instability threshold is different among different models. For models close to the threshold, changing the amount of freshwater input in the North Atlantic, as a consequence of global warming, may lead to a collapse of the THC and the shift to an equilibrium with no water sinking in the North Atlantic (Ganopolsky et al. 2001, their Fig. 11).

6. Conclusions

We analyzed the sensitivity of the climate to diapycnal diffusivity for the equilibrium climate state. We focused particularly on the behavior of the THC and on vertical heat balance in the ocean. Additionally, a sensitivity study on the hysteresis cycle of the THC to the diapycnal diffusion is conducted with the MIT EMIC. This study is unique because the sensitivity to diapycnal diffusion of the ocean has been investigated using a coupled model with a 3D ocean component.

For the present climate state, the strength of the THC in the North Atlantic scales with the 0.44 power of the diapycnal diffusivity whereas a simple theoretical model predicts a power of 2/3. The theoretical model assumes a vertical–diffusive balance in the ocean. Since the Pacific Ocean is about twice as large as the Atlantic Ocean most of the upwelling likely occurs in the former basin. Indeed, in our model, the Southern Pacific overturning scales with the 0.63 power of the diapycnal diffusivity. Hence, a factor that may be related to the THC strength in the Pacific, for a climate close to equilibrium, is the value of the diapycnal diffusivity in the Pacific basin.

At equilibrium, the vertical heat balance of the global ocean is sensitive to the diapycnal diffusivity. Weaker mixing in the ocean leads to smaller diapycnal diffusive fluxes in the Tropics and a thinner thermocline. As a consequence, isopycnal slopes at high latitudes are gentler, leading to smaller isopycnal diffusive and bolus advective fluxes. Although the THC strength sensibly depends on the value of the diapycnal diffusivity, compensation between high latitude downwelling and tropical upwelling leads to small changes of the total vertical advective flux. The relative importance of the fluxes at high latitude, compared to the fluxes in the tropical region, depends on the diapycnal diffusivity—the main cause being the reduction of diapycnal diffusion in the Tropics. For elevated diapycnal diffusivity, the Tropics dominate the global balance and the advective-diffusive balance is valid at all depths. For reduced diapycnal diffusivity, high latitude processes are relatively more important than low latitude ones and, for the global ocean, the advective–diffusive balance is reversed in the upper 800 m.

In addition, we performed a sensitivity test of the hysteresis curve to the diapycnal diffusivity. As suggested by previous studies with coupled 2D multibasin ocean models and a 3D uncoupled ocean model the THC becomes more unstable to freshwater perturbations for lower values of the diapycnal diffusivity. In 3D ocean models, the threshold for the shutdown of the THC depends on the diapycnal diffusivity, while in coupled 2D multibasin ocean models, the same threshold is relatively insensitive to the diapycnal diffusivity. Less clear is the sensitivity of the threshold at which the circulation recovers from the "shutdown" mode. In the 3D uncoupled model of Prange et al. (2003) the above threshold slightly increases with decreasing diapycnal diffusivity. The opposite occurs for the MIT EMIC and the coupled 2D multibasin ocean models. The gyre transport of salt in the North Atlantic, the atmosphere-

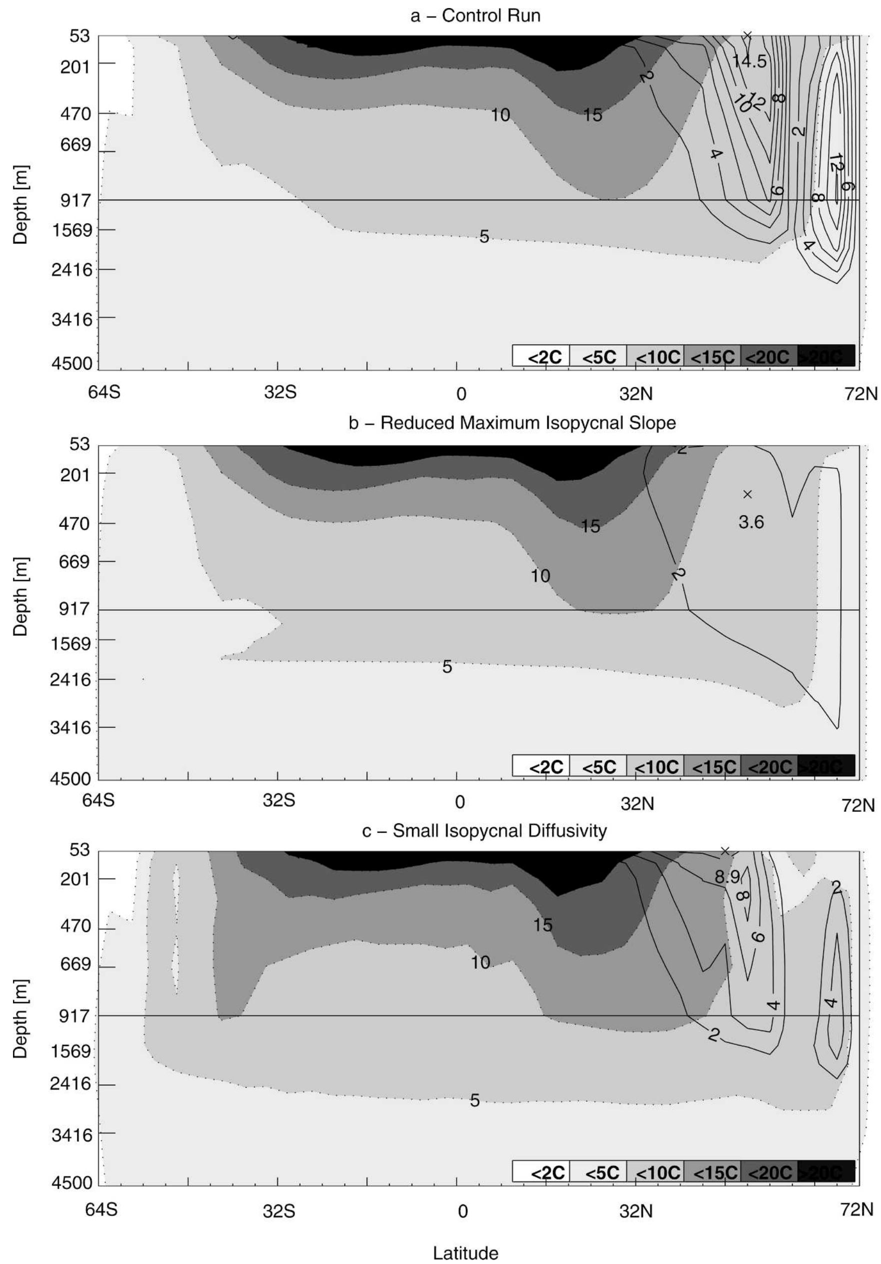

FIG. A1. Bolus velocity streamfunction in the Atlantic Ocean for diapycnal diffusivity 0.5 $cm^2 s^{-1}$: (a) control run, (b) reduced maximum isopycnal slope, and (c) small isopycnal diffusivity experiments. Zonal average temperature is shaded according to the scale in (a).

ocean feedbacks and the nonlinear dynamics are the major differences among the above models.

Acknowledgments. We thank the two anonymous reviewers for useful comments and suggestions that improved the clarity of the manuscript. This research was supported in part by MIT's Joint Program on the Science and Policy of Global Change and in part by the Office of Science (BER), U.S. Department of Energy, Grant DE-FG02-93ER61677.

APPENDIX

A Convectionless Model

Convection in this version of the MIT EMIC is almost negligible. In models with horizontal and vertical diffusion parameterizations convection is the only means by which heat can be transported efficiently from the deep ocean to the surface. With the recent introduction of Redi and Gent–McWilliams parameter-

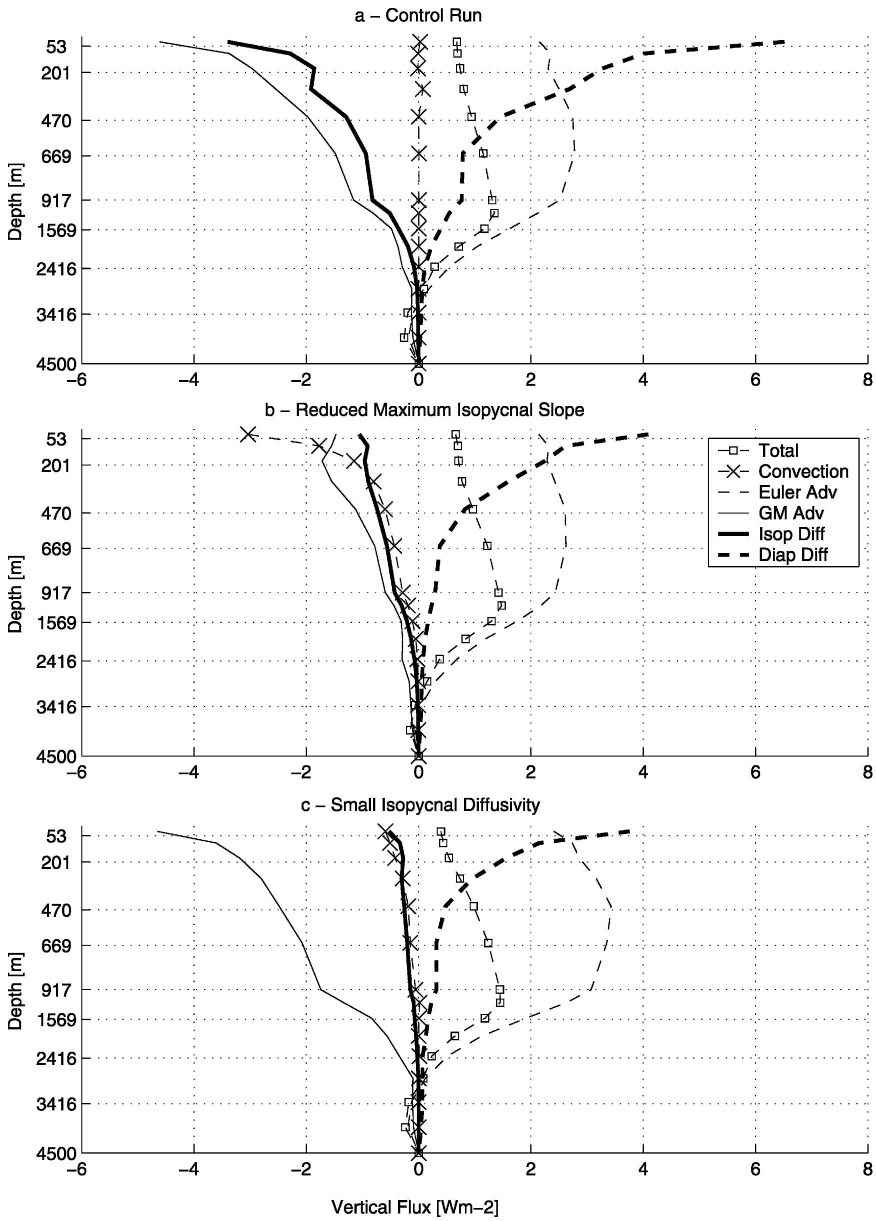

FIG. A2. Vertical heat balance in the Atlantic Ocean for diapycnal diffusivity 0.5 $cm^2 s^{-1}$: (a) control run, (b) reduced maximum isopycnal slope, and (c) small isopycnal diffusivity experiments.

izations (Redi 1982; Gent and McWilliams 1990), both isopycnal mixing and bolus velocities can efficiently mix the upper ocean, inhibiting convection. This effect has been noticed already in 2D (Harvey 1995, their Fig. 2) and 3D ocean models (Danabasoglu and McWilliams 1995, their Fig. 22). In our model steeply sloping isopycnals are eliminated by using the tapering method of Gerdes et al. (1991), with a maximum slope of 0.01.

Reducing the isopycnal mixing and/or the bolus velocities would increase the ocean heat content and reduce the static stability. Convection should then be enhanced. To prove that this is the case, we have performed two additional equilibrium experiments. From the control run with diapycnal diffusion 0.5 $cm^2 s^{-1}$, we spun up the coupled model in a separate experiment with the upper bound on the isopycnal slopes reduced from 0.01 in the standard model to 0.001, and in another experiment with the isopycnal diffusivity reduced from 1000 to 100 $m^2 s^{-1}$.

In the reduced maximum slope (RMS) case, the maximum overturning in the Atlantic increases 2 Sv in comparison with the standard model (26 Sv), while the temperature structure is almost unchanged. Moreover, the GM streamfunction is reduced in the Southern Ocean but almost canceled in the North Atlantic, going from a maximum of 15 Sv to less that 4 Sv (Figs. A1a,b).

In the small isopycnal diffusion (SID) case, the maximum overturning in the North Atlantic decreases by 2 Sv and the whole ocean warms up. The GM streamfunction is reduced by about 4 Sv, against the 11-Sv reduction of the RMS case (Figs. A1a,c). The introduction of the GM mixing scheme has been shown in the past to improve the representation of the ocean circulation mainly in the Southern Ocean (Danabasoglu and McWilliams 1995, their Figs. 4 and 5), thus a distribution of the bolus velocities as in the RMS case, with larger velocities in the Southern Ocean than in the Northern Ocean, agrees better with that reported in 3D GCMs with realistic geometry (Danabasoglu and McWilliams 1995).

The heat balance of the Atlantic Ocean only is presented in Fig. A2. In the RMS case both the isopycnal diffusive flux and GM advective flux are about half the control run fluxes (Figs. A2a,b). Compensating the reduction of these fluxes, a reduction of diapycnal diffusive fluxes and the appearance of upward convective fluxes are observed. Eulerian advection is virtually unchanged. In the SID case, the isopycnal diffusive fluxes decrease considerably, balancing the reduction of diapycnal diffusion (Figs. A2a,c). Convection plays a minor but not negligible role in the balance, while Eulerian advection slightly increases at every depth level.

This result confirms that convective fluxes in the standard version of our model are being inhibited by GM advective fluxes and isopycnal diffusive fluxes. Greatly reducing the isopycnal diffusion only allows for convection to constitute a small term in the heat balance. However, reducing both isopycnal diffusion and GM advection by roughly 50% (accomplished by reducing the maximum slope of isopycnals) strongly enhances convective mixing. Therefore, we suggest that the GM fluxes are more efficient than the isopycnal fluxes in increasing the stability of the water column. Changing the isopycnal diffusivity and the maximum isopycnal slope involves also changes in the circulation pattern as well as in the surface heat flux distribution.

REFERENCES

Bryan, F., 1987: Parameter sensitivity of primitive equation ocean general circulation models. *J. Phys. Oceanogr.,* **17,** 970–985.

Bryan, K., 1984: Accelerating the convergence to equilibrium of ocean–climate models. *J. Phys. Oceanogr.,* **14,** 666–673.

Claussen, M., and Coauthors, 2002: Earth system models of intermediate complexity: Closing the gap in the spectrum of climate system models. *Climate Dyn.,* **18,** 579–586.

Colin de Verdière, A., 1988: Buoyancy driven planetary flows. *J. Mar. Res.,* **46,** 215–265.

Cummins, P. F., G. Holloway, and A. E. Gargett, 1990: Sensitivity of the GFDL ocean general circulation model to a parameterization of vertical diffusion. *J. Phys. Oceanogr.,* **20,** 817–830.

Dalan, F., P. H. Stone, and A. P. Sokolov, 2005: Sensitivity of the ocean's climate to diapycnal diffusivity in an EMIC. Part II: Global warming scenario. *J. Climate,* **18,** 2482–2496.

Danabasoglu, G., and J. C. McWilliams, 1995: Sensitivity of the global ocean circulation to parameterizations of mesoscale tracer transports. *J. Climate,* **8,** 2967–2987.

Ganachaud, A., and C. Wunsch, 2003: Large-scale ocean heat and freshwater transports during the World Ocean Circulation Experiment. *J. Climate,* **16,** 696–705.

Ganopolsky, A., V. Petoukhov, S. Rahmstorf, V. Brovkin, M. Claussen, A. Eliseev, and C. Kubatzki, 2001: CLIMBER-2: A climate system model of intermediate complexity. Part II: Model sensitivity. *Climate Dyn.,* **17,** 735–751.

Gent, P. R., and J. C. McWillams, 1990: Isopycnal mixing in ocean circulation models. *J. Phys. Oceanogr.,* **20,** 150–155.

Gerdes, R., C. Köberle, and J. Willebrand, 1991: The influence of numerical advection schemes on the results of ocean general circulation models. *Climate Dyn.,* **5,** 211–226.

Gnanadesikan, A., 1999: A simple predictive model for the structure of the ocean pycnocline. *Science,* **283,** 2077–2079.

Gregory, J. M., 2000: Vertical heat transports in the ocean and their effect on time-dependent climate change. *Climate Dyn.,* **16,** 501–515.

Griffies, S. M., A. Gnanadesikan, R. C. Pacanowski, V. D. Larichev, J. K. Dukowicz, and R. D. Smith, 2000: Spurious diapycnal mixing associated with advection in a *z*-coordinate ocean model. *Mon. Wea. Rev.,* **128,** 538–564.

Hansen, J., G. Russel, D. Rind, P. Stone, A. Lacis, S. Lebedeff, R. Ruedy, and L. Travis, 1983: Efficient three-dimensional global models for climate studies: Model I and II. *Mon. Wea. Rev.,* **111,** 609–662.

Harvey, L. D. D., 1995: Impact of isopycnal diffusion on heat fluxes and the transient response of a two-dimensional ocean model. *J. Phys. Oceanogr.,* **25,** 2166–2176.

Houghton, J. T., Y. Ding, D. J. Griggs, M. Noguer, P. J. van der Linden, X. Dai, K. Maskell, and C. A. Johnson, 2001: *Climate Change 2001: The Scientific Basis.* Cambridge University Press, 881 pp.

Huang, B., P. H. Stone, and C. Hill, 2003: Sensitivities of deep-ocean heat uptake and heat content to surface fluxes and subgrid-scale parameters in an ocean general circulation model with idealized geometry. *J. Geophys. Res.,* **108,** 3015, doi:10.1029/2001JC001218.

Huang, R. X., 1999: Mixing and energetics of the oceanic thermohaline circulation. *J. Phys. Oceanogr.,* **29,** 727–746.

Hughes, T. C. M., and A. J. Weaver, 1994: Multiple equilibria of an asymmetric two-basin ocean model. *J. Phys. Oceanogr.,* **24,** 619–637.

Jiang, S., P. H. Stone, and P. Malanotte-Rizzoli, 1999: An assessment of the GFDL ocean model with course resolution. Part I: Annual mean climatology. *J. Geophys. Res.,* **104,** 25 623–25 646.

Kamenkovich, I. V., J. Marotzke, and P. H. Stone, 2000: Factors affecting heat transport in an ocean general circulation model. *J. Phys. Oceanogr.,* **30,** 175–194.

——, A. P. Sokolov, and P. H. Stone, 2002: An efficient climate model with a 3D ocean and a statistical-dynamical atmosphere. *Climate Dyn.,* **19,** 585–598.

Klinger, B. A., S. Drijfhout, J. Marotzke, and J. R. Scott, 2003: Sensitivity of basinwide meridional overturning to diapycnal diffusion and remote wind forcing in an idealized Atlantic–Southern Ocean geometry. *J. Phys. Oceanogr.,* **33,** 249–266.

Knutti, R., T. F. Stocker, and D. Wright, 2000: The effects of subgrid-scale parameterizations in a zonally averaged ocean model. *J. Phys. Oceanogr.,* **30,** 2738–2752.

Ledwell, J. R., E. T. Montgomery, K. L. Polzin, L. C. St. Laurent, R. W. Schmitt, and J. M. Toole, 2000: Evidence for enhanced mixing over rough topography in the abyssal ocean. *Nature,* **403,** 179–182.

Levitus, S., and T. P. Boyer, 1994: *Temperature*. Vol. 4, *World Ocean Atlas 1994*, NOAA Atlas NESDIS 4, 117 pp.

Manabe, S., and R. J. Stouffer, 1994: Multiple-century response of a coupled ocean–atmosphere model to an increase of atmospheric carbon dioxide. *J. Climate,* **7,** 5–23.

Marotzke, J., 1997: Boundary mixing and the dynamics of three-dimensional thermohaline circulation. *J. Phys. Oceanogr.,* **27,** 1713–1728.

——, and J. R. Scott, 1999: Convective mixing and the thermohaline circulation. *J. Phys. Oceanogr.,* **29,** 2962–2970.

——, and B. A. Klinger, 2000: The dynamics of equatorially asymmetric thermohaline circulations. *J. Phys. Oceanogr.,* **30,** 955–970.

Munk, W., 1966: Abyssal recipes. *Deep-Sea Res.,* **13,** 707–730.

——, and C. Wunsch, 1998: Abyssal recipes. Part II: Energetics of tidal and wind mixing. *Deep-Sea Res.,* **45,** 1977–2010.

Pacanowski, R. C., 1996: MOM2 version 2.0: Documentation user's guide and reference manual. Geophysical Fluid Dynamics Laboratory Tech. Rep. 3.2, 232 pp.

Park, Y. G., and K. Bryan, 2000: Comparison of thermally driven circulations from a depth-coordinate model and an isopycnal-layer model. Part I: Scaling-law sensitivity to vertical diffusivity. *J. Phys. Oceanogr.,* **30,** 590–605.

Polzin, K. L., J. M. Toole, J. R. Ledwell, and R. W. Schmitt, 1997: Spatial variability of turbulent mixing in the abyssal ocean. *Science,* **276,** 93–96.

Prange, M., G. Lohmann, and A. Paul, 2003: Influence of vertical mixing on the thermohaline hysteresis: Analyses of an OGCM. *J. Phys. Oceanogr.,* **33,** 1707–1721.

Prinn, R., and Coauthors, 1999: Integrated global system model for climate policy assessment: Feedbacks and sensitivity studies. *Climatic Change*, **41,** 469–546.

Rahmstorf, S., 1995: Bifurcations of the Atlantic thermohaline circulation in the response to changes in the hydrological cycle. *Nature,* **378,** 145–149.

Redi, M. H., 1982: Oceanic isopycnal mixing by coordinate rotation. *J. Phys. Oceanogr.,* **12,** 1154–1158.

Samelson, R. M., 1998: Large-scale circulation with locally enhanced vertical mixing. *J. Phys. Oceanogr.,* **28,** 712–726.

Schmittner, A., and A. J. Weaver, 2001: Dependence of multiple climate states on ocean mixing parameters. *Geophys. Res. Lett.,* **28,** 1027–1030.

Scott, J. R., 2000: The role of mixing and geothermal heating and surface buoyancy forcing in ocean meridional overturning dynamics. Ph.D. thesis, Massachusetts Institute of Technology, 128 pp.

——, and J. Marotzke, 2002: The location of diapycnal mixing and the meridional overturning circulation. *J. Phys. Oceanogr.,* **32,** 3578–3595.

Sokolov, A. P., and P. H. Stone, 1998: A flexible climate model for use in integrated assessments. *Climate Dyn.,* **14,** 291–303.

Stone, P. H., and M.-S. Yao, 1990: Development of a two-dimensional zonally averaged statistical–dynamical model. Part III: The parameterization of the eddy fluxes of heat and moisture. *J. Climate,* **3,** 726–740.

Thorpe, R. B., J. M. Gregory, T. C. Johns, R. A. Woods, and J. F. B. Mitchell, 2001: Mechanisms determining the Atlantic thermohaline circulation response to greenhouse gas forcing in a non-flux-adjusted coupled climate model. *J. Climate,* **14,** 3102–3116.

Toggweiler, J. R., and B. Samuels, 1995: Effect of Drake Passage on the global thermohaline circulation. *Deep-Sea Res.,* **42,** 477–500.

Vallis, G. K., 2000: Large-scale circulation and production of stratification: Effects of wind, geometry, and diffusion. *J. Phys. Oceanogr.,* **30,** 933–954.

Welander, P., 1971: The thermocline problem. *Philos. Trans. Roy. Soc. London,* **270A,** 415–421.

Wright, D. G., and T. F. Stocker, 1992: Sensitivities of a zonally averaged global ocean circulation model. *J. Geophys. Res.,* **97,** 12 707–12 730.

Zhang, J., 1998: Impacts of double-diffusive processes on the thermohaline circulation. Ph.D. thesis, Massachusetts Institute of Technology and Woods Hole Oceanographic Institution, 157 pp.

——, R. W. Schmitt, and R. X. Huang, 1999: The relative influence of diapycnal mixing and hydrologic forcing on the stability of the thermohaline circulation. *J. Phys. Oceanogr.,* **29,** 1096–1108.

Sensitivity of the Ocean's Climate to Diapycnal Diffusivity in an EMIC. Part II: Global Warming Scenario

FABIO DALAN, PETER H. STONE, AND ANDREI P. SOKOLOV

Joint Program on the Science and the Policy of Climate Change, Massachusetts Institute of Technology, Cambridge, Massachusetts

(Manuscript received 9 April 2004, in final form 15 December 2004)

ABSTRACT

The sensitivity of the ocean's climate to the diapycnal diffusivity in the ocean is studied for a global warming scenario in which CO_2 increases by 1% yr^{-1} for 75 yr. The thermohaline circulation slows down for about 100 yr and recovers afterward, for any value of the diapycnal diffusivity. The rates of slowdown and of recovery, as well as the percentage recovery of the circulation at the end of 1000-yr integrations, are variable, but a direct relation with the diapycnal diffusivity cannot be found. At year 70 (when CO_2 has doubled) an increase of the diapycnal diffusivity from 0.1 to 1.0 $cm^2\ s^{-1}$ leads to a decrease in surface air temperature of about 0.4 K and an increase in sea level rise of about 4 cm. The steric height gradient is divided into thermal component and haline component. It appears that, in the first 60 yr of simulated global warming, temperature variations dominate the salinity ones in weakly diffusive models, whereas the opposite occurs in strongly diffusive models.

The analysis of the vertical heat balance reveals that deep-ocean heat uptake is due to reduced upward isopycnal diffusive flux and parameterized-eddy advective flux. Surface warming, induced by enhanced CO_2 in the atmosphere, leads to a reduction of the isopycnal slope, which translates into a reduction of the above fluxes. The amount of reduction is directly related to the magnitude of the isopycnal diffusive flux and parameterized-eddy advective flux at equilibrium. These latter fluxes depend on the thickness of the thermocline at equilibrium and hence on the diapycnal diffusion. Thus, the increase of deep-ocean heat uptake with diapycnal diffusivity is an indirect effect that the latter parameter has on the isopycnal diffusion and parameterized-eddy advection.

1. Introduction

Climate models are very sensitive to the diapycnal diffusivity, both for the equilibrium climate state (Bryan 1987; Marotzke 1997; Zhang et al. 1999; Park and Bryan 2000) and in transient experiments, triggering strong nonlinear behavior (Ganopolsky et al. 2001; Manabe and Stouffer 1999). Yet, the global averaged value of the diapycnal diffusivity is uncertain. Measurements of the diapycnal diffusivity are localized in space and time (Polzin et al. 1997; Ledwell et al. 2000) while calculations of the global averaged diapycnal diffusivity vary as much as a factor 5 (Munk and Wunsch 1998; Huang 1999). In Part I of this study we analyzed the sensitivity of the current climate to the diapycnal diffusivity (Dalan et al. 2005). In this paper we illustrate the influence of the diapycnal diffusivity on the transient behavior of the thermohaline circulation (THC) and on the rate of change of heat content, sea surface temperature, and sea level rise.

The THC appears to be driven by the steric height gradient between North and South Atlantic (Hughes and Weaver 1994). By changing the relative strength of the processes transporting heat and salt in the ocean, positive feedbacks may strengthen, triggering strong nonlinear behavior in the THC evolution. By changing the rate of CO_2 increase in the atmosphere, Stocker and Schmittner (1997) observed a slowdown and recovery of the THC or a complete collapse of the THC for slow and fast rates respectively. The same pattern was observed by Ganopolsky et al. (2001), varying both vertical diffusivity and hydrological sensitivity in a 2D multibasin ocean model coupled with a 2D statistical-dynamical model. For low vertical diffusivity and high hydrological sensitivity, the THC shuts down in a simulation with 1% CO_2 rate of increase for 140 yr and constant afterward (stabilization at 4 × CO_2). For all

Corresponding author address: Fabio Dalan, Via Cavour 44/e, 35030 Rubano (PD), Italy.
E-mail: fabio.dalan@alum.mit.edu

the other combinations of the two parameters the strength of the THC decreases for about 150 yr and then partially recovers. This study will extend Ganopolsky et al. (2001) results by using a 3D ocean model coupled with a 2D atmosphere and varying only the diapycnal diffusivity. Furthermore, the change in steric height gradient is divided into thermal component and haline component and the relative magnitude of the components is analyzed with respect to changes in the diapycnal diffusivity.

In the last Intergovernmental Panel on Climate Change (IPCC) report (Houghton et al. 2001), the results from model projections of leading research groups are presented. Among other quantities, models are commonly compared in terms of surface air temperature (SAT) change and sea level rise (SLR). All models simulate an increase in surface air temperature and sea level, as a consequence of an increase of CO_2 in the atmosphere, but the magnitude of the increase varies as much as a factor of three. Both SAT and SLR due to thermal expansion depend on the rate of deep-ocean heat uptake. The rate of increase of SAT depends on the effective heat capacity of the Earth system. Because of the large heat capacity of water compared to air and land, the heat capacity of the combined atmosphere–land–ocean system depends on the portion of ocean that will be affected by global warming, therefore on the rate of ocean heat uptake. The sea level rises mainly because the volume of the water increases with temperature; therefore, it also depends on the rate at which the ocean takes up heat.

The rate of ocean heat uptake is not well constrained by observations of the temperature record of the past 50 yr (Forest et al. 2002) and varies greatly among models (Sokolov et al. 2003). Hence, detailed studies on the vertical heat balance in the ocean are needed in order to understand which processes and parameters control the rate of ocean heat uptake in numerical models. Two studies of this kind are presented by Gregory (2000) and Huang et al. (2003c). In the first study advective fluxes (Eulerian and parameterized-eddy velocity advection) and diffusive fluxes (isopycnal and diapycnal) are combined together, when analyzing the global ocean balance, and the balance for different latitude bands and basins is limited to a single depth level (160 m). We will hereafter refer to the parameterized-eddy advective flux as the GM flux from the commonly used Gent–McWilliams parameterization (Gent and McWilliams 1990). Huang et al. (2003a,b,c) combine together the isopycnal diffusive flux and the GM flux. Their adjoint sensitivity studies show that the heat content of the ocean and its change in transient climate scenarios is dependent on these combined fluxes (Huang et al. 2003a,b). However, varying both the isopycnal and thickness diffusivities simultaneously does not change appreciably the rate of ocean heat uptake (Huang et al. 2003c). In this paper, the vertical heat flux of the ocean is divided into all its components and for every depth level. Moreover the sensitivity of the rate of deep-ocean heat uptake to diapycnal diffusivity is presented for a standard global warming scenario. For the sensitivity of the vertical heat balance at equilibrium refer to Dalan et al. (2005).

Uncertainty in the heat uptake is a major source of uncertainty in global warming projections (Webster el al. 2003). Sokolov et al. (2003) found that the difference in the heat uptake simulated by coupled atmosphere–ocean GCMs (AOGCMs) could be described by differences in the rate at which heat anomalies are effectively diffused into the ocean. Using the Sokolov et al. (2003) model to fit the trend of the Massachusetts Institute of Technology (MIT) earth model of intermediate complexity (EMIC), we will relate the diapycnal diffusivity to the effective vertical diffusivity of Sokolov et al. (2003).

The paper is organized as follows: in section 2 we briefly describe the numerical model; in section 3 we analyze the transient behavior of the THC circulation for simulations with different diapycnal diffusivity; section 4 contains the sensitivity of the ocean heat uptake, SAT and SLR to the diapycnal diffusivity; finally, section 5 contains a review of the results.

2. MIT earth model of intermediate complexity

More details of the model can be found in Kamenkovich et al. (2002).

a. Atmospheric component

The two-dimensional zonally averaged statistical-dynamical atmospheric model was developed by Sokolov and Stone (1998) on the basis of the Goddard Institute for Space Studies (GISS) GCM (Hansen et al. 1983). The model solves the zonally averaged primitive equations in latitude-pressure coordinates. The grid of the model consists of 24 points in the meridional direction, corresponding to a resolution of 7.826°, and nine layers in the vertical. Moreover, the model includes the parameterization of heat, moisture and momentum transports by large-scale eddies (Stone and Yao 1990) and has a complete moisture and momentum cycle.

Most of the physics and parameterizations of the atmospheric model derive from the GISS GCM. The 2D model, as well as the GISS GCM, allows four different types of surfaces in the same grid cell, namely, open ocean, sea ice, land, and land ice. The surface characteristics, as well as turbulent and radiative fluxes, are calculated separately for each kind of surface, while the atmosphere above is assumed to be well-mixed zonally. The atmospheric model uses a realistic land/ocean ratio at each latitude band. More detailed description of this part of the model can be found in Sokolov and Stone (1998) and Prinn et al. (1999).

The dependence of zonal-mean surface fluxes of heat and momentum on surface warming simulated by this model coupled to a 2D ocean model is similar to that shown by more sophisticated atmospheric GCMs (Sokolov and Stone 1998; Prinn et al. 1999). Moreover, vertical and latitudinal structure of the 2D model response is also consistent with the results of different GCMs. However, such a model cannot represent feedbacks associated with changes in the ocean circulation. To take into account possible interactions between atmosphere and ocean circulation, the 2D ocean model is replaced, in this study, by a 3D ocean GCM with simplified geometry.

b. *Ocean component*

The ocean component of the coupled model is the modular ocean model (MOM2; Pacanowski 1996) with idealized geometry. It consists of two rectangular "pool" basins connected by a Drake Passage that extends from 64° to 52°S. The Indo-Pacific (hereinafter Pacific) pool extends from 48°S to 60°N and is 120° wide while the Atlantic pool extends from 48°S to 72°N and is 60° wide. The meridional resolution is 4° and the zonal resolution varies from 1° near the north–south boundaries to 3.75° in the interior of the ocean. In the vertical, the model has 15 layers of increasing thickness from 53 m at the surface to 547 m at depth. The bottom of the ocean is flat and 4500 m deep everywhere except in the Drake Passage where there is a sill 2900 m deep.

No-slip boundary conditions are applied to the lateral walls and free-slip boundary conditions at the bottom of the ocean, except in the Antarctic Circumpolar Current (ACC) where bottom drag is applied so as to obtain a more realistic speed for the ACC. Boundary conditions for tracers are insulating at lateral walls and bottom of the ocean. A mixed layer model adopted from the GISS GCM replaces the ocean GCM southward of 64°S and northward of 72°N. The depth of the mixed layer is prescribed from observations as a function of latitude and time. In climate change simulations, heat penetrating into the ocean below the mixed layers is parameterized by diffusion of the deviation of the mixed layer temperature from its present-day climate values. Moreover, any changes in the runoff are evenly distributed throughout the ocean at any given time.

The Gent–McWilliams parameterization scheme is used to account for the small-scale eddy induced transport (Gent and McWilliams 1990). Mixing caused by small-scale processes occurs along and across isopycnals (Redi 1982). No background horizontal diffusivity is used. The surface boundary conditions used to spin up the ocean model are taken from Jiang et al. (1999) who constructed the datasets using a variety of sources.

c. *Coupling, spinup, and experimental setup*

Coupling takes place twice a day. The atmospheric model calculates 12-h mean values of the wind stress, heat, and freshwater fluxes over the open ocean and their derivatives with respect to the SST. These quantities are then linearly interpolated to the oceanic grid. The derivatives of the surface fluxes with respect to the SST are multiplied by the deviation of the SST from its zonal mean. This term is then added to the atmospheric surface fluxes and passed to the ocean model. This procedure allows one to account for the zonal variations of the surface fluxes. The coupling procedure uses flux adjustments. The adjustments are given by the difference between the surface fluxes diagnosed after the spinup of the ocean-only model and the fluxes generated in the spinup of the atmospheric model alone forced by observed SST and sea ice distribution. The ocean is integrated for 12 h and provides to the atmosphere the zonal mean SST. Asynchronous integration is used (Bryan 1984), with 12 h time step for the tracer equations and 1 h time step for the momentum equations. For more details on the coupling procedure see Dalan et al. (2005) and Kamenkovich et al. (2002).

After separate spinup of the atmospheric and oceanic components the model has been coupled and spun up for 1000 yr for each value of the diapycnal diffusivity: 0.1, 0.2, 0.5, and 1.0 $cm^2\ s^{-1}$. The model was considered to be at equilibrium when the global average heat flux entering the ocean fluctuates around the zero value. In the global warming experiments, the CO_2 in the atmosphere increases by 1% yr^{-1} for 75 yr and then it is kept constant for 925 yr. Control runs are also performed starting at the end of the coupled spinup, with constant CO_2 concentration for 1000 yr. As a measure of the transient climate change at the time of CO_2 doubling we take the difference between the mean climate in the global warming experiments and the control climate averaged over years 66–75.

3. Behavior of the thermohaline circulation

In our model the thermohaline circulation slows down as a consequence of enhanced CO_2 in the atmo-

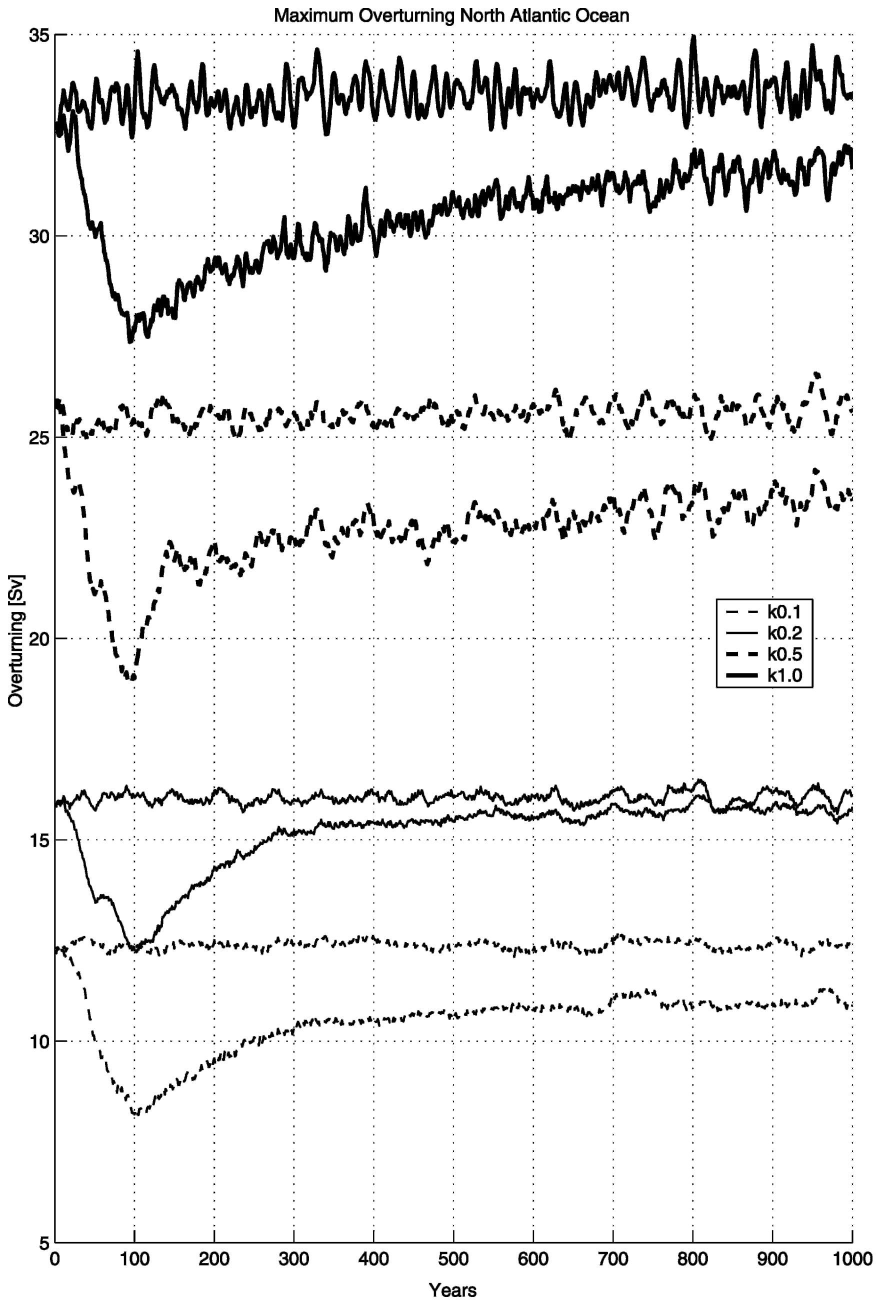

FIG. 1. Maximum meridional streamfunction in the North Atlantic Ocean. For each value of the diapycnal diffusivity, both control experiment and global warming overturning strength is displayed. The control overturning strength of the THC fluctuates around a mean value that depends on the diapycnal diffusivity. In global warming experiments the THC strength diminishes for about 100 yr and then partially or fully recovers its original value. Diffusivity 0.1 $cm^2\ s^{-1}$, thin dashed line; 0.2 $cm^2\ s^{-1}$, thin solid line; 0.5 $cm^2\ s^{-1}$, thick dashed line; and 1.0 $cm^2\ s^{-1}$, thick solid line.

sphere (Fig. 1), as it does in most CMIP2 (Coupled Model Intercomparison Project) models. For each global warming simulation with different diapycnal diffusivity, the strength of circulation in the Atlantic Ocean decreases for 100 yr, 25 yr after the stabilization of the CO_2, and it recovers afterward. Hence, the behavior of the system to changes in diapycnal diffusivity is self-similar. Ganopolsky el al. (2001) found strong nonlinear behavior of the THC varying both vertical diffusivity and hydrological sensitivity.[1] For small vertical diffusivity and large hydrological sensitivity the THC shuts down for a 1% CO_2 increase for 140 yr, while for all other combinations of the two parameters the THC slows down and then partially recovers. Our model is extremely stable to freshwater perturbations, as inferred from the hysteresis curves presented in Dalan et al. (2005). Moreover, we do not register major changes in freshwater flux in the North Atlantic as a consequence of global warming (Kamenkovich et al. 2003).

The rate and the amount of recovery vary for each experiment in an unpredictable way. For example, the simulation with diffusivity 0.5 $cm^2\ s^{-1}$ presents the fastest recovery although it is with the diffusivity 0.2 $cm^2\ s^{-1}$ that the circulation first fully recovers its strength (Fig. 1). Moreover, the natural variability of the THC in the control run increases with the diapycnal diffusivity, its value going from 0.2 Sv for the 0.1 $cm^2\ s^{-1}$ diffusivity to 1 Sv for the 1.0 $cm^2\ s^{-1}$ diffusivity. The behavior of the circulation depicted in Fig. 1 raises the question of the predictability of the THC in global warming experiments (Knutti and Stocker 2002). Regardless of the path followed in the recovery, the new equilibrium achieved after the CO_2 stabilization, presents a shallower overturning circulation (not shown), as noted by Huang et al. (2003c). As a consequence of the THC slowdown, the bottom of the ocean fills up with cold water, which represents an obstacle for the water sinking in the North Atlantic when the circulation recovers. Little changes are registered in the rate of Antarctic Bottom Water (AABW) formation. This may be due to our model configuration as extending the Drake Passage all the way to Antarctica inhibits the AABW formation in ocean GCMs with idealized topography (Hughes and Weaver 1994).

The steric height is the integrated pressure from the surface to a reference depth; hence, it is proportional to the quantity

$$P = \int_{z*}^{0} \int_{z}^{0} \frac{\rho}{\rho_o} dz'\, dz,$$

where ρ is the in situ density, ρ_0 is a reference density and $z*$ is a reference depth, in our case 3000 m. The THC strength at equilibrium is correlated to the steric height difference between the North and South Atlantic (Hughes and Weaver 1994; Thorpe et al. 2001). In the idealized geometry of the MIT EMIC, the steric height difference is not sensitive to the choice of the south Atlantic latitude, as long as the latter is located northward of the Drake Passage, while the North Atlantic latitude needs to be north of 60°N. The THC strength at equilibrium is best correlated to the steric height difference in the Atlantic Ocean when the latter is calculated between 30°S and 66°–70°N. Since the THC circulation is stronger for increasing diapycnal diffusivity, the gulf stream extends to higher latitudes for models with 0.5 and 1.0 $cm^2\ s^{-1}$ diapycnal diffusivity. Hence, for a fair comparison among simulations with different diapycnal diffusivity, the steric height is calculated between 30°S and 66°N for diffusivities 0.1 and 0.2 $cm^2\ s^{-1}$ and between 30°S and 70°N for diffusivities 0.5 and 1.0 $cm^2\ s^{-1}$.

Both the percentage reduction of the THC strength and steric height gradient decrease with increasing overturning (Fig. 2). However, the steric height gradient change does not correlate with the percentage recovery at the end of the integration. This indicates that the longitudinal variations of the steric height may be relevant to explain the transient behavior of the THC.

Since the steric height depends on the density of the water column, we want to quantify the relative importance of the temperature and salinity profile in determining the steric height gradient. Using the temperature field from the transient run and the salinity field from the control run, we can calculate the temperature contribution to the steric height gradient. The salinity contribution is computed with the same technique. The result is depicted in Fig. 3. For all simulations, the time series of the temperature and salinity contribution to the steric height gradient anomaly have a common trend, summarized as follows: at first, both temperature and salinity contributes to the decrease of the steric height gradient, while, after a certain time, temperature and salinity have opposite contributions to the steric height gradient (Fig. 3). The time at which the rate of change of the salinity contribution becomes positive is roughly 140 yr for the smallest diffusivities (0.1 and 0.2 $cm^2\ s^{-1}$) and 70 yr for the largest diffusivities (0.5 and 1.0 $cm^2\ s^{-1}$). Therefore we can identify two types of systems: a slow responding system for small diffusivities and a fast responding system for large diffusivities.

An important characteristic of the response of the system is the relative role of temperature and salinity in determining the steric height gradient in the first 75 yr of the transient runs. For slow responding systems, the temperature effect is always the dominant term (Figs. 3a,b). For fast responding systems, in the first decades of integration, the salinity anomalies have greater importance (Figs. 3c,d) than the temperature anomalies in determining the steric height gradient. At the time of

[1] The hydrological sensitivity allows one to regulate the amount of freshwater flux into the North Atlantic.

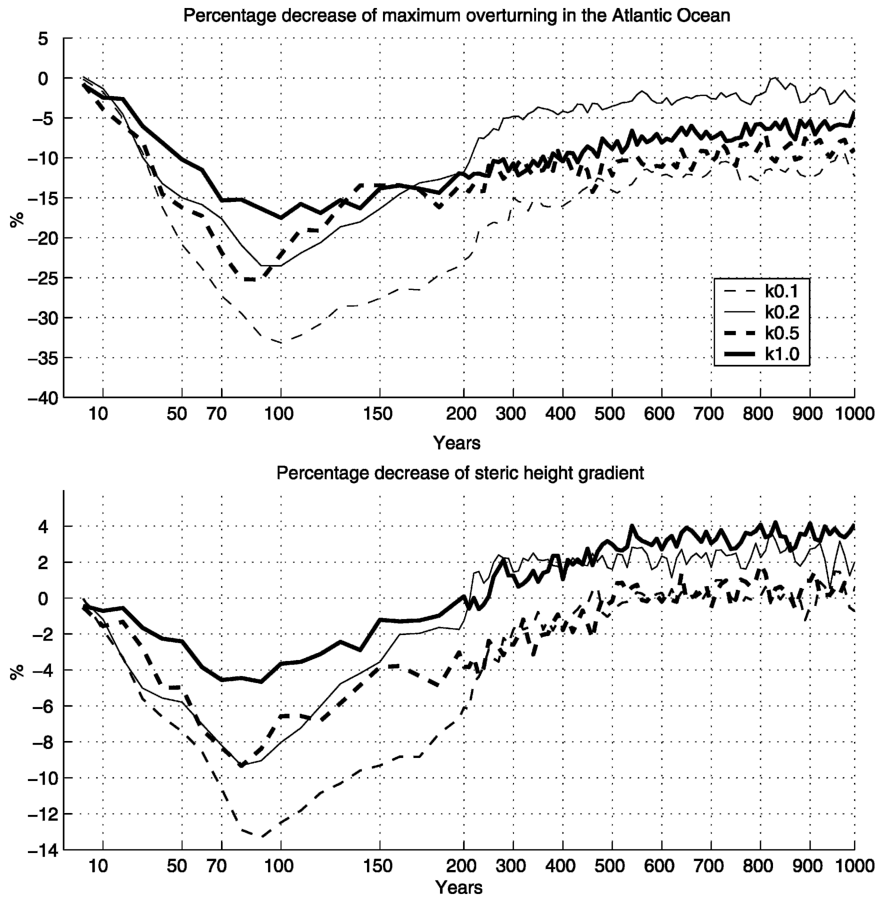

FIG. 2. Percentage reduction of (top) maximum meridional streamfunction and (bottom) steric height gradient in the Atlantic Ocean for different values of the diapycnal diffusivity: diffusivity 0.1 cm^2 s^{-1}, thin dashed line; 0.2 cm^2 s^{-1}, thin solid line; 0.5 cm^2 s^{-1}, thick dashed line; and 1.0 cm^2 s^{-1}, thick solid line. Note the stretching of the horizontal axis.

doubling of CO_2 however, the changes in the temperature distribution in the ocean are driving the steric height gradient for all the global warming simulations.

Thorpe et al. (2001) carried out a detailed analysis of the changes in steric height gradient. The authors concluded that, in the first 70 yr of global warming, at the surface fluxes of heat and freshwater tend to slowdown the THC, while the changes in the meridional heat and salt transport help the THC recovery. An examination of our results suggests that the salinity fluxes in the deep ocean are dominated by advection, both in the equilibrium and transient experiments. For the temperature contribution the situation is more complicated. Changes in the GM advection and isopycnal diffusion tend to warm the North Atlantic, as we will see in the next section. Moreover, the reduction of the THC implies a substantial reduction of the heat transport into high latitudes. This leads to a relative cooling of the North Atlantic and warming of the tropical Atlantic. Hence, changes in both GM advection and isopycnal diffusion decrease the steric height gradient while the decrease in meridional heat transport tends to increase it. Additionally, the density contribution of the heat flux at the surface in the North Atlantic in our model is about 7 times larger than the freshwater flux as shown by Kamenkovich et al. (2003, their Figs. 2a and 3).

The climate is a potentially chaotic system, therefore the realizations portrayed in Fig. 3 may depend on the initial condition. To further investigate this aspect, we perform another global warming experiment with diapycnal diffusivity 0.5 cm^2 s^{-1} starting from year 10 of the control run. Starting from a different initial condition slightly changes the relative importance of temperature and salinity in the first 70 yr of integration (not shown). In particular, in one case the salt component of the steric height anomaly is larger than the temperature component for about 65 yr of global warming; in the

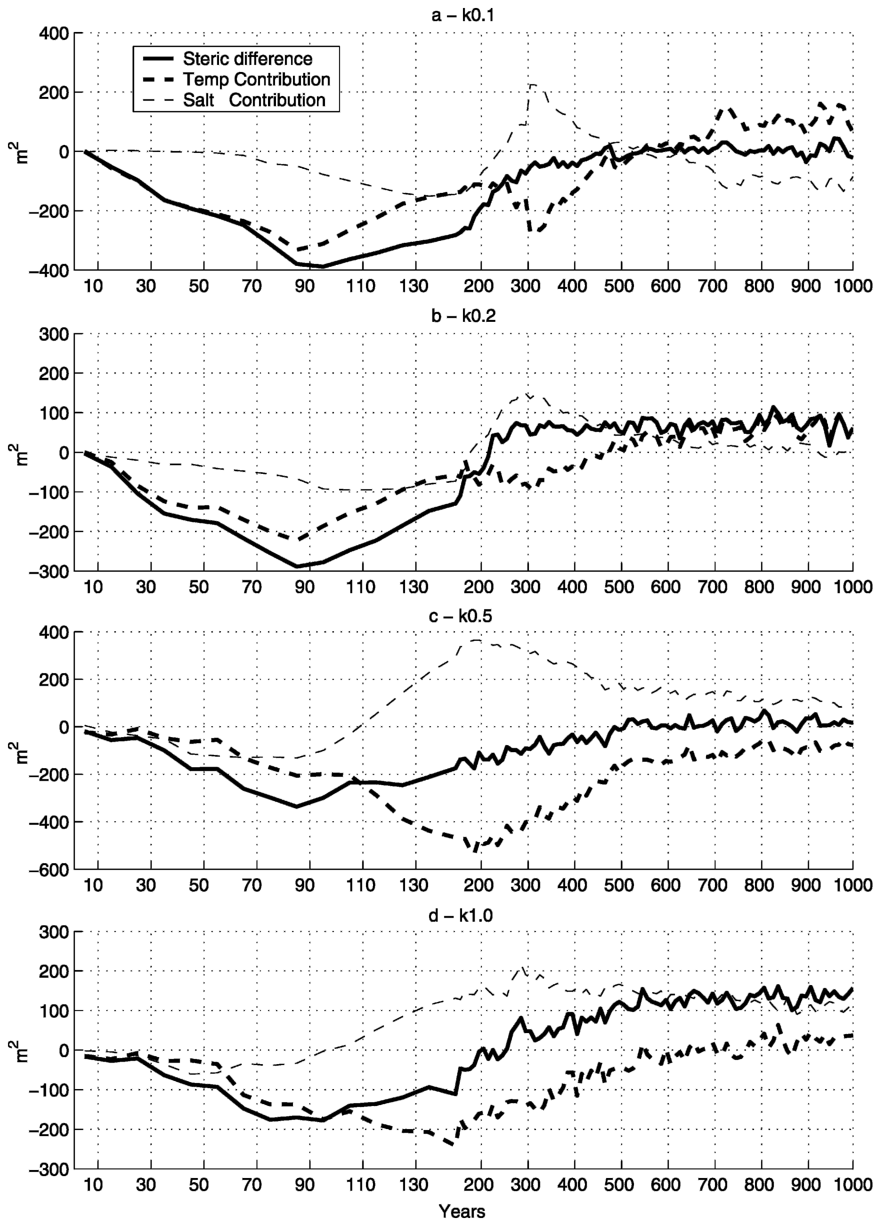

FIG. 3. Steric height gradient anomaly (solid) and its temperature (thick dashed) and salinity (thin dashed) contribution in the Atlantic Ocean for different values of the diapycnal diffusivity: (a) 0.1, (b) 0.2, (c) 0.5, and (d) 1.0 $cm^2\ s^{-1}$. Note the stretching of the horizontal axis.

other case the dominance of the salt component extends shortly over 70 yr of integration.

A direct consequence of our observations is that models with large equilibrium THC overturning may be more sensitive to changes in the salt content in the North Atlantic, as a consequence of enhanced CO_2 in the atmosphere. Hence, even for models showing the same surface heat and freshwater flux perturbations under global warming experiments, the sensitivities to the surface forcing may be different.

4. Vertical heat imbalance

The ocean heat uptake is an important factor in controlling the behavior of the THC under global warming experiments because it affects the temperature, and therefore the density, structure of the ocean. Hence, investigating the relationship between ocean heat uptake and diapycnal diffusivity may give some insight on the behavior of the THC under global warming experiments. In the previous section we have seen how the competition between temperature and salinity, in determining the steric height gradient, is affected by the diapycnal diffusivity. Here, we investigate which processes are responsible for the temperature change in the deep ocean as the CO_2 increases in the atmosphere, and what is their relation with respect to the diapycnal diffusivity. Addressing these questions can help us understand whether differences in diapycnal diffusivity is one reason for the disagreement among IPCC models in the matter of surface air temperature and sea level rise. We are interested in the different contributions of advection and diffusion to the global ocean vertical heat flux. Local contributions of the vertical heat flux components are presented in order to show how the contribution to the global balance varies from a region to another. We do not include the meridional heat flux components as they do not affect the global heat balance and their discussion goes beyond the purpose of this study. We note however that the storage in the individual regions is small compared to the individual flux convergences, and thus the total meridional flux convergences almost cancel the total vertical flux convergences in the individual regions.

a. Global warming experiment

In our global warming experiments the global ocean warms above 2500 m and cools below this level (Fig. 4a). Cooling at depth occurs in the Northern Ocean (Fig. 4b) and it is due to the reduction of the THC, with consequent reduction of downward advective heat transport in the North Atlantic. The reduction of upwelling in the Tropics (Fig. 4c) compensates for the reduction of heating so that changes in the advective heat flux for the global ocean are small (Fig. 4a).

Heating in the upper 2500 m is due to a decrease in both upward isopycnal diffusion and GM advection and it is concentrated at high latitudes (Figs. 4b,d), in agreement with the adjoint sensitivity study of Huang et al. (2003b, their Fig. 5). Surface heating in global warming experiments leads to less steep isopycnal slopes, which explain the decrease in GM flux. Moreover, with increasing temperature, the density field becomes more dependent on the temperature field, because of the nonlinear dependence of the expansion coefficients on temperature and salinity. Hence, the angle between isopycnals and isotherms decreases, leading to a decrease of isopycnal temperature gradient and lastly of the isopycnal flux, as noted by Gregory (2000).

Surface warming leads to greater vertical temperature gradient and increased diapycnal diffusion in the tropical region (Fig. 4c). On the other hand, in dynamically active regions like the Northern and Southern Ocean the downward diapycnal flux decreases compensating the decrease of the upward isopycnal flux (Figs. 4b,d). As pointed out in Dalan et al. (2005, their Fig. 10), the heat balance at the high latitudes has isopycnal diffusion and diapycnal diffusion acting in the same locations. Isopycnal diffusion removes heat from the deep ocean, thus tending to increase the vertical temperature gradient, while diapycnal diffusion tends to relax this gradient by pumping heat downward. A similar tendency to compensate occurs in global warming experiments: reduction of isopycnal fluxes leads to warming at depth and a relatively small vertical temperature gradient, which then leads to a decrease in the downward diapycnal diffusion.

In Fig. 5, the heat flux anomalies for the Northern Ocean and the Tropics are separated for the Atlantic and Pacific basins. It is clear that the Northern Ocean anomalous fluxes are representative of the North Atlantic (Figs. 5a,b). The area-integrated diapycnal flux anomaly in the tropical Pacific is about 3 times as large as in the tropical Atlantic because the area coverage of the Pacific is twice the Atlantic's; however, the decreased upwelling in the Tropics is greater in the tropical Atlantic than in the tropical Pacific (Figs. 5c,d).

The analysis of vertical heat fluxes in a global warming experiment is also presented by Gregory (2000). At 160-m depth the anomalous fluxes consist of: reduction of convection in the Northern Ocean, reduction of upwelling in the tropical region and reduction of upward isopycnal diffusion in the Southern Ocean. The total heat flux anomaly in the Southern Ocean and Tropics are respectively 0.55 and 0.59 Wm^{-2}, more that three times the anomaly in the Northern Ocean (0.16 Wm^{-2}).

Qualitatively our results agree with Gregory (2000) in the Tropics and in the Northern Ocean, allowing for the fact that in this model the role of convection is replaced by GM advection and isopycnal diffusion (Dalan et al. 2005). In the Southern Ocean we find that reduction of both isopycnal diffusion and GM advection are the major contributors to the increased heat flux. Quantitatively, we note that the vertical heat balance sensibly depends on depth (Fig. 4). At high latitudes, the global heat flux anomaly decreases with depth from a value of 0.5 Wm^{-2} at the surface (Figs. 4b,d). At the Tropics the anomaly is roughly constant at 0.2 Wm^{-2} between the surface and 2000 m, then decreasing with depth until the bottom of the ocean (Fig. 4c). Therefore, above 400 m both Northern and Southern Oceans contribute the most to the global heat flux anomaly, while below this level the Tropics present the highest anomaly.

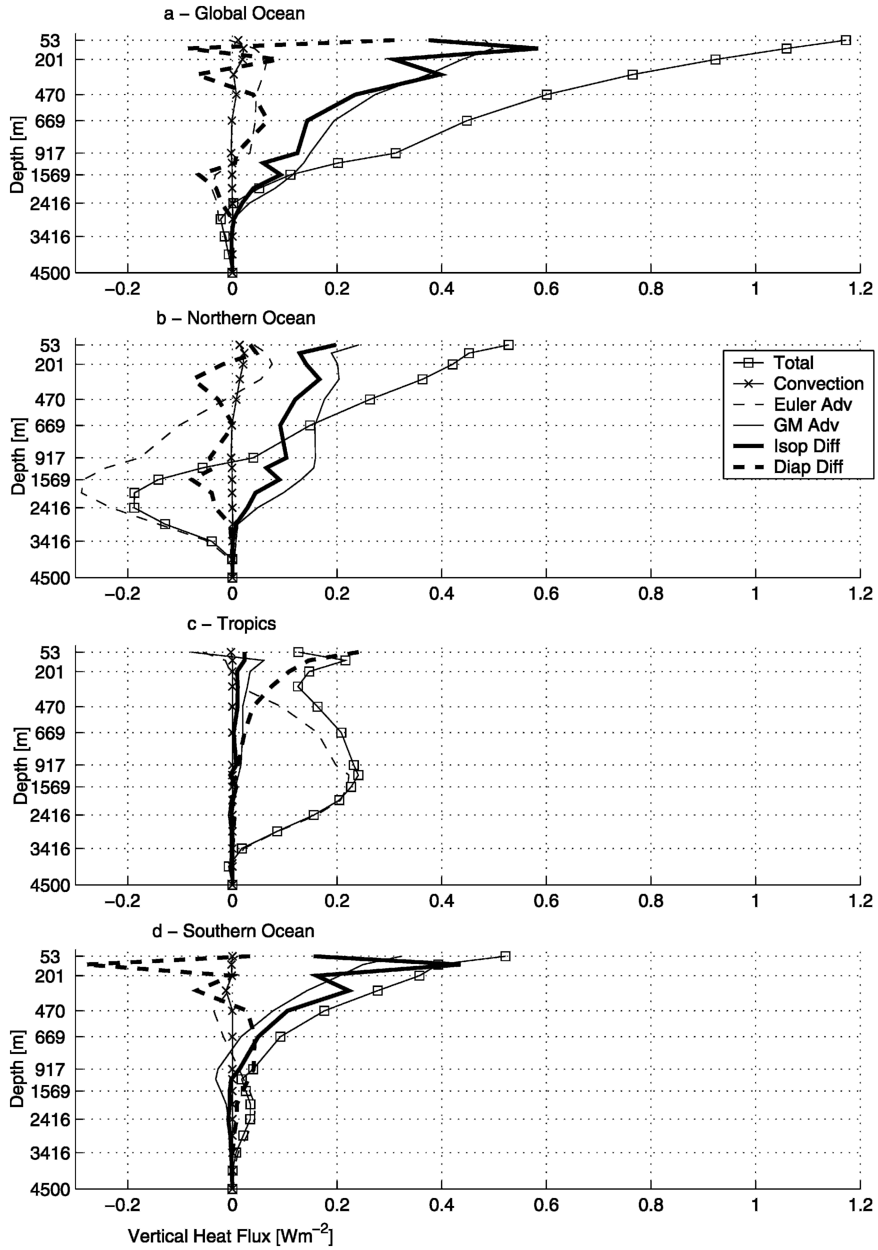

FIG. 4. Global warming experiment. Vertical heat flux anomalies for (a) global ocean, (b) Northern Ocean, (c) Tropics, and (d) Southern Ocean for diapycnal diffusivity 0.5 $cm^2 s^{-1}$, averaged from years 66–75 of simulation. Positive (negative) sign indicates increase (decrease) for downward fluxes or decrease (increase) for upward fluxes with respect to equilibrium. Upward fluxes are isopycnal diffusion, GM advection, and convection. Downward fluxes are advection and diapycnal diffusion.

b. Sensitivity to diapycnal diffusion

Because the anomalous isopycnal and GM fluxes are the main contributors to the total anomalous heat flux (Fig. 4a), it is natural to think that, by changing isopycnal and/or thickness diffusivities, the amount of heat penetrating the ocean would change accordingly. This is not the case as Huang et al. (2003c) found. Employing the same configuration of the MIT EMIC used in this study,[2] the authors changed both isopycnal and thickness diffusivities by a factor of 2. The anomalous

[2] The MIT Ocean Model code was used instead of MOM2.

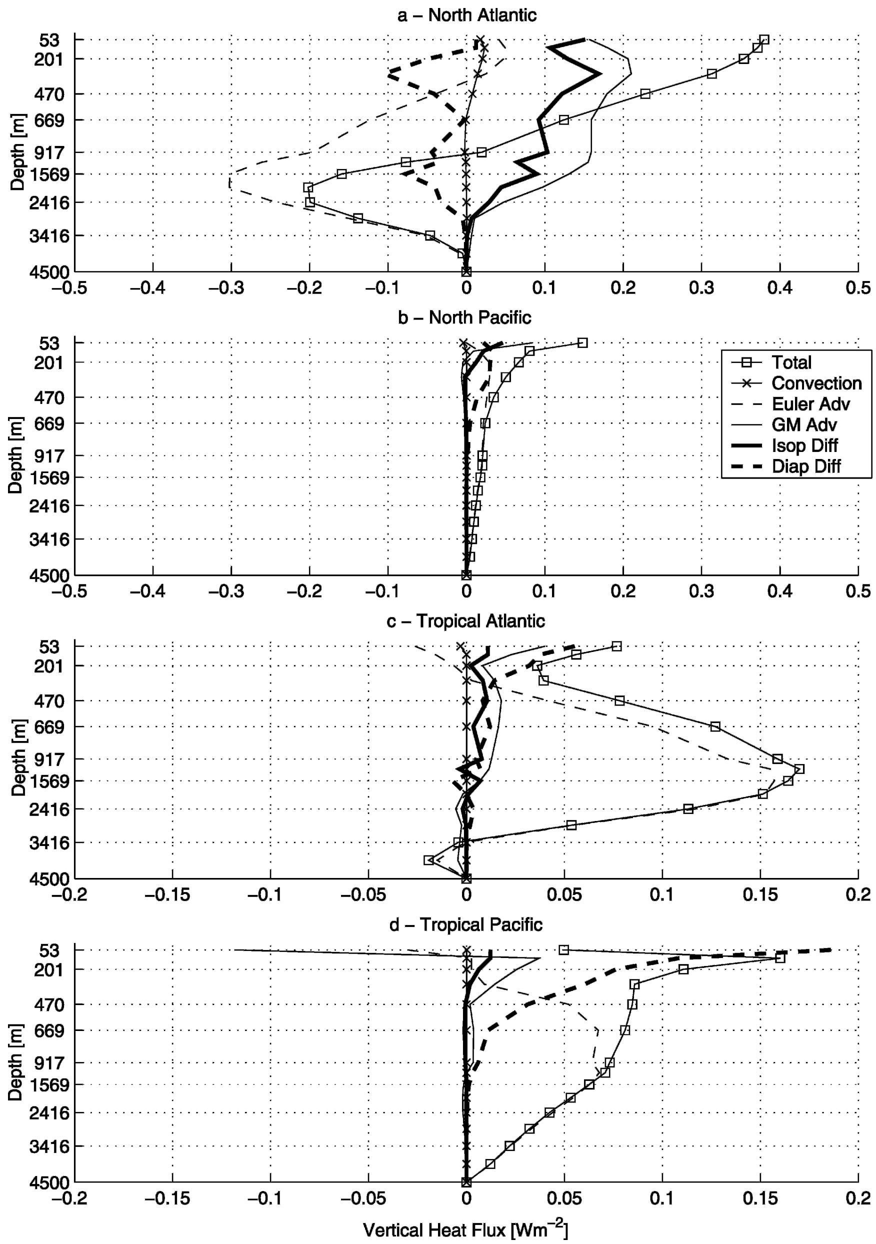

FIG. 5. Global warming experiment, as in Fig. 4, but for vertical heat flux anomalies of the (a) North Atlantic, (b) North Pacific, (c) tropical Atlantic, and (d) tropical Pacific for diapycnal diffusivity 0.5 $cm^2 s^{-1}$, averaged from years 66–75 of simulation.

heat flux from isopycnal diffusion and GM advection varied, although only slightly, in the same direction as the parametric change (their Fig. 11), and the total anomalous heat flux did not vary appreciably. The same does not happen when the diapycnal diffusion changes, since the total anomalous heat flux entering the ocean sensibly increases at all depths as the diapycnal diffusion increases (Fig. 6).

In global warming simulations the anomalous fluxes behave in the same way for all simulations given varying diapycnal diffusivity (Fig. 6). The major contributions to the heat uptake by the ocean are due to the reduction of isopycnal and GM fluxes at all depths. The magnitude of the total anomaly is directly proportional to the diffusivity, implying a greater heat penetration for high diapycnal diffusivity (Fig. 6). The reason for the increase is not directly related to the increase of diffusive heat from the ocean surface, as common physical intuition might suggest. Maximum warming is localized at high latitudes of the Atlantic Basin and in

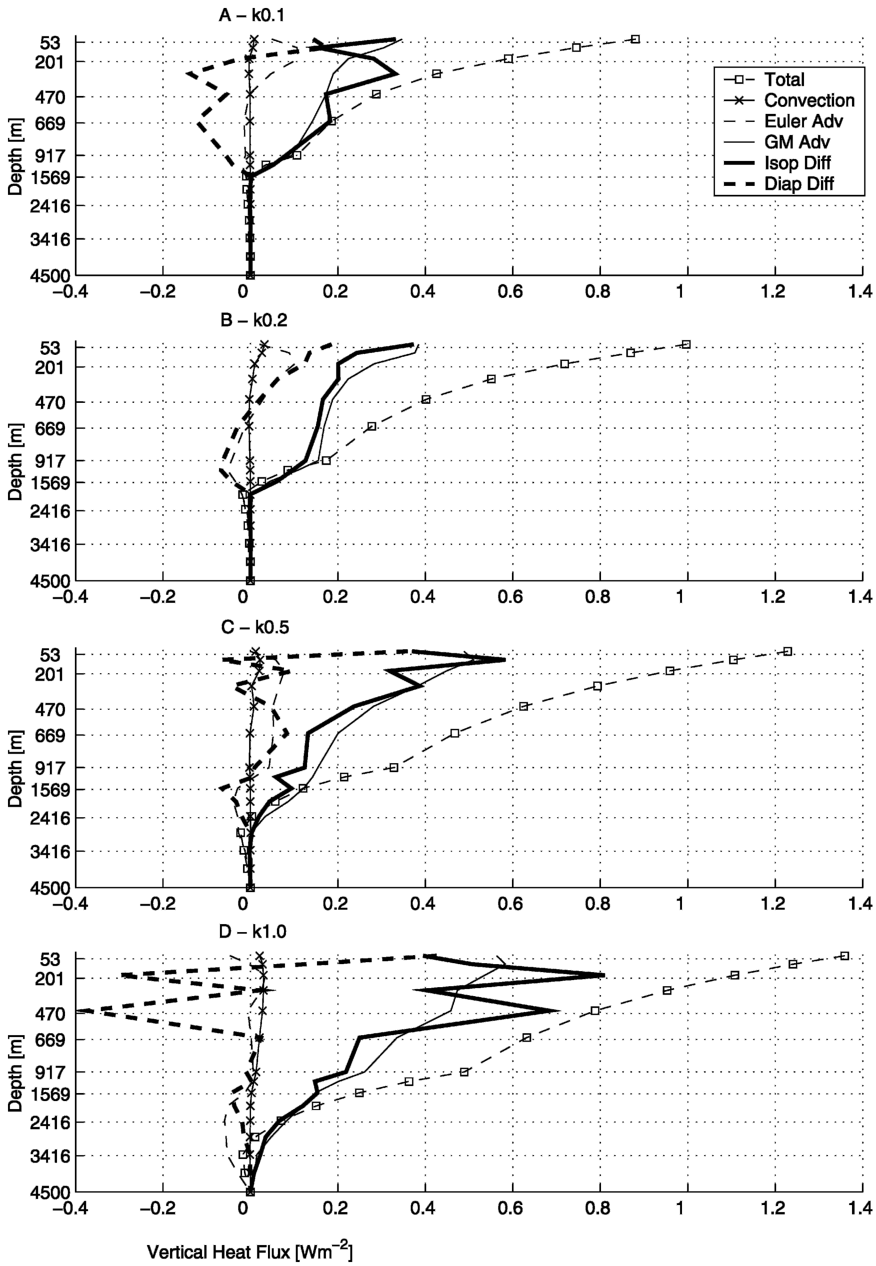

FIG. 6. Changes in vertical heat fluxes due to global warming for the global ocean and for diapycnal diffusivity (a) 0.1, (b) 0.2, (c) 0.5, and (d) 1.0 cm^2 s^{-1}, averaged from years 66–75 of simulation. Positive (negative) sign indicates increase (decrease) for downward fluxes or decrease (increase) for upward fluxes with respect to equilibrium. Upward fluxes are isopycnal diffusion, GM advection, and convection. Downward fluxes are advection and diapycnal diffusion.

the Southern Ocean (Fig. 7), where isopycnal diffusion and GM advection dominate, both in magnitude in the control runs (Dalan et al. 2005) and in tendency in global warming experiments (Fig. 6). Note that the relative small warming at 50°N in the Atlantic basin (Fig. 7) is caused by a southward shift of the Gulf Stream, as a consequence of the slowdown of the Thermohaline Circulation.

The connection between elevated diapycnal diffusivity and ocean heat uptake, given by isopycnal diffusion and GM advection, is found in the temperature structure of the ocean in the control run. The thickness of

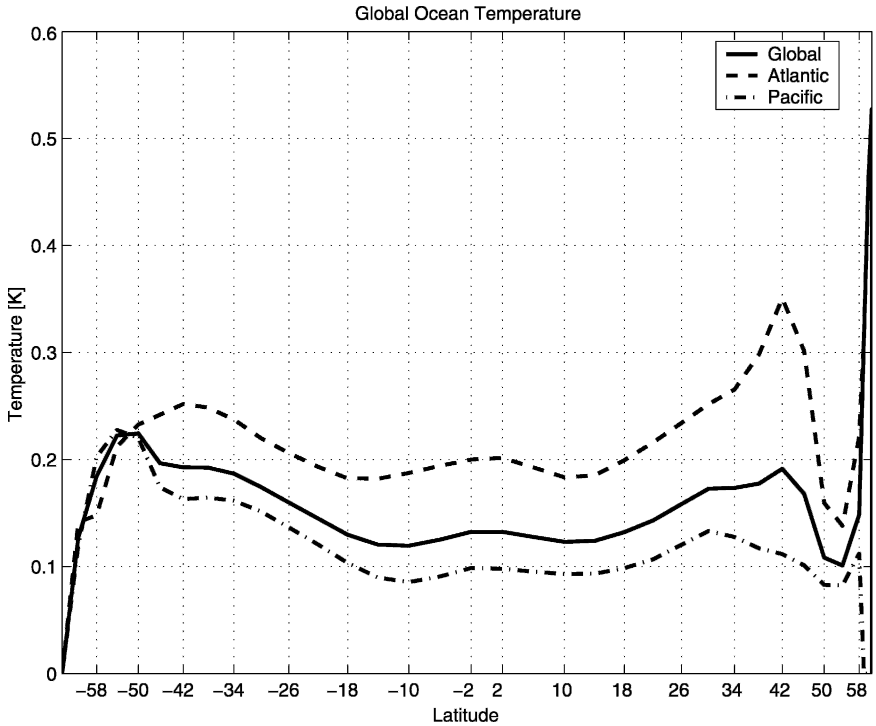

FIG. 7. Meridional distribution of global ocean temperature anomaly at the time of CO_2 doubling for diapycnal diffusivity 0.5 $cm^2\ s^{-1}$.

the thermocline is proportional to the diapycnal diffusivity, due to the larger heat diffusion from the surface of the ocean. Hence, at high latitudes the isopycnal slope increases as the thermocline deepens, followed by an increase of isopycnal and GM fluxes.[3] In global warming simulations, the surface warming reduces the isopycnal slopes in high latitudes of the North Atlantic (Fig. 8) leading to a decrease of upward GM and isopycnal fluxes. The magnitude of the decrease is proportional to their control values, hence to the thickness of the thermocline and lastly to the diapycnal diffusivity. We recall that in this version of the MIT EMIC, the role of convection is inhibited by the efficient mixing caused by isopycnal diffusion and GM advection. If the maximum isopycnal slope is reduced, convection plays a significant role in the vertical heat balance at equilibrium (Dalan et al. 2005, their Fig. A2) and possibly also under global warming experiments.

c. Comparison with CMIP2

In simulations with a 1% yr^{-1} increase in CO_2 concentration, performed as part of the coupled model intercomparison project (see online at http://www-pcmdi.llnl.gov/cmip.cmiphome.html), the increase in global mean SAT at the time of CO_2 doubling ranged from 1.32 to 2.15°C (Covey et al. 2000) for different models. Similarly the results for SLR due to thermal expansion of the ocean ranged from 6.5 to 14.5 cm (S. Raper 2000, personal communication). The different model responses are associated with differences in the models' effective climate sensitivity and rate of heat uptake. Sokolov et al. (2003) showed that changes in the global mean SAT and SLR simulated by different AOGCMs can be reproduced by the MIT 2D climate model (Sokolov and Stone, 1998) with an appropriate choice of the 2D model's climate sensitivity and its rate of heat uptake in the ocean. The latter is simulated by diffusing heat anomalies into the deep ocean with an effective global mean diffusion coefficient, K_υ, which represents the net effect of all oceanic processes: advection, diffusion and convection.

Sensitivity experiments showed little dependence of the total heat uptake by the ocean on the isopycnal diffusivity and GM parameter when the latter are varied together (Huang et al. 2003c). Moreover, to the lowest order, advection by the THC is directly proportional to the diapycnal diffusivity. Hence, we can expect a strong relationship between K_υ and the diapycnal dif-

[3] At equilibrium all fluxes increase for increasing diapycnal diffusion (Dalan et al. 2005, their Fig. 11).

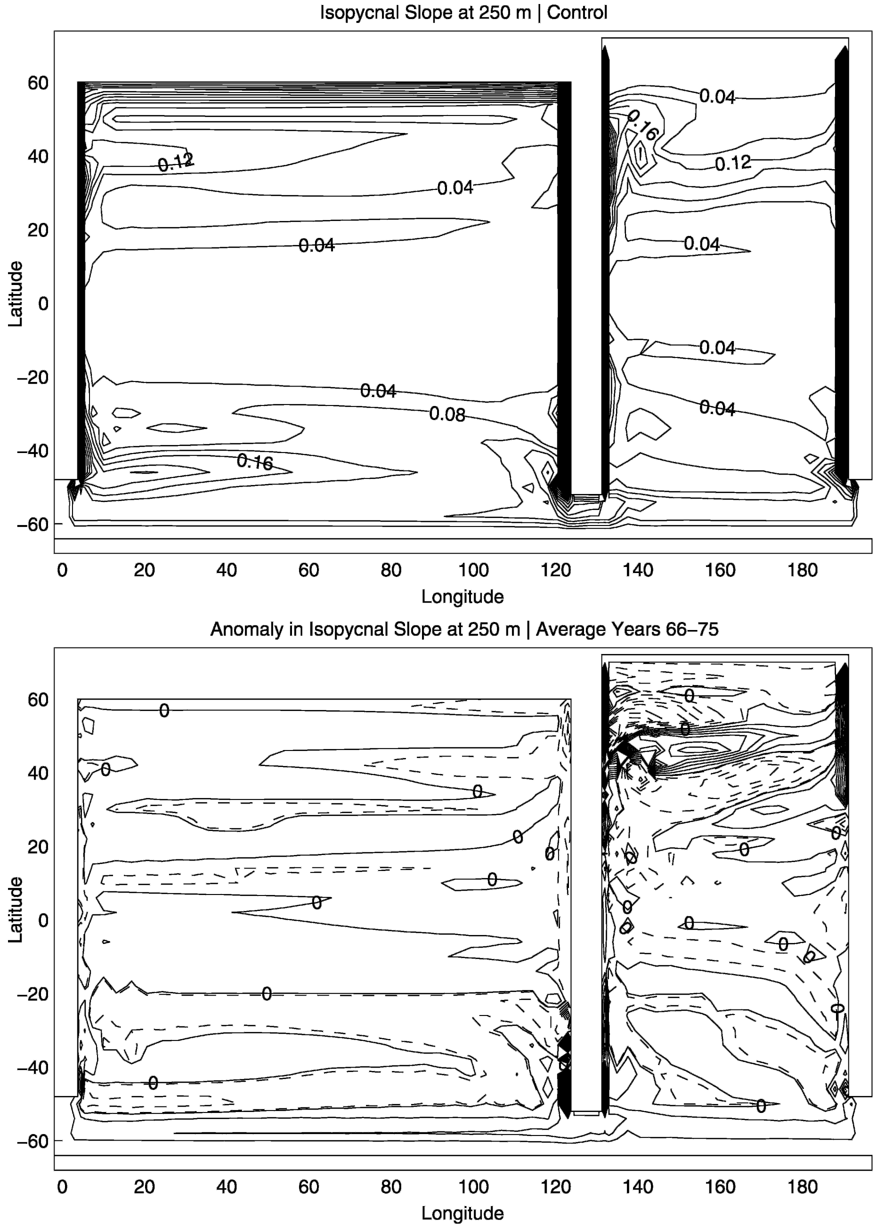

FIG. 8. Modulus of the (top) isopycnal slope and (bottom) its anomaly due to global warming at 250-m depth for diapycnal diffusivity 0.5 $cm^2 s^{-1}$. Solid line denotes positive values and dashed line denotes negative values.

fusivity. Indeed in our GCM we can vary the ocean heat uptake by varying the diapycnal diffusivity (Fig. 6).

This diapycnal mixing parameter mimics the effect of processes such as the wind stirring at the surface of the ocean and the internal waves, mostly induced by the breaking of tidal waves over the bottom topography. Numerical models make use of different parameterization schemes to account for the spatial variations of the diapycnal mixing, while, for the sake of simplicity and to aid our understanding of the experimental results, we chose a uniform diapycnal diffusivity. Quantity such as SAT and SLR depend on the effective diffusivity K_v, and our results help us to understand the differences among CMIP2 models.

Table 1 shows how varying the diapycnal mixing coefficient from 0.1 to 1.0 $cm^2 s^{-1}$ changes the response of our model. The different responses of the model give an estimate of the uncertainty in global warming projections due to uncertainty in the diapycnal diffusion. Table 1 also gives the values of K_v in the 2D model that

TABLE 1. Model results at year 70 in the global warming scenario. (b) Surface air temperature anomaly, (c) sea level rise due to thermal expansion at the time of doubling CO_2, and (d) effective diffusivity of the MIT 2D climate model in global warming experiments with (a) different diapycnal diffusivity.

a	Diapycnal diffusivity ($cm^2\ s^{-1}$)	0.1	0.2	0.5	1.0
b	Change in SAT (K)	1.83	1.68	1.57	1.46
c	SLR (cm)	9.2	10.3	12.1	13.1
d	Equivalent K_υ ($cm^2\ s^{-1}$)	5.0	7.5	37	125

allow it to mimic the response of our model for different values of the diapycnal diffusivity. These values of K_υ cover most of the range of the CMIP2 models, which goes from 4 to 50 $cm^2\ s^{-1}$ (Sokolov et al. 2003, their Fig. 1). Thus the MIT-EMIC with varying values of the diapycnal diffusivity can also be used in sensitivity studies where the effect of different rates of oceanic heat uptake need to be taken into account (Webster et al. 2003). We note that the range of values for the change in SAT and SLR shown in table 1 are not as large as for the CMIP2 models, because the MIT EMIC results shown in Table 1 are for a fixed climate sensitivity of 2.8 K, whereas the climate sensitivity of the CMIP2 models ranges from 1.9 to 4.2 K.

5. Conclusions

We analyzed the sensitivity of the climate to diapycnal diffusivity for a global warming scenario focusing on the behavior of the THC and on the rate of heat uptake by the ocean. This study is the first to explore the sensitivity to diapycnal diffusion of the ocean using a coupled model with a 3D ocean component.

Increasing the carbon dioxide level in the atmosphere at a rate of 1% yr^{-1} for 75 yr leads to a slowdown of the THC circulation for about 100 yr and recovery afterward. The rate at which the circulation recovers and the percentage recovery at the end of the simulation vary with the diapycnal diffusion in an unpredictable fashion. For the largest (1.0 $cm^2\ s^{-1}$) and smallest (0.1 $cm^2\ s^{-1}$) values of the diapycnal diffusivity, recovery is slow and incomplete at the end of the 1000 yr integration. For diapycnal diffusivity equal to 0.5 $cm^2\ s^{-1}$ the circulation recovers rapidly, while for diapycnal diffusivity equal to 0.2 $cm^2\ s^{-1}$ the circulation first recovers completely its control strength. For the first 60–70 yr of integration, what differentiates the response of the climate system (as the diapycnal diffusion varies) is the relative contribution of temperature and salinity in determining the evolution of steric height gradient between North and South Atlantic. In climate systems with small diapycnal diffusivity, the temperature variations largely explain the changes in steric height gradient, while in highly diffusive ocean models, the salinity variations are comparable to the temperature's in terms of steric height. Thus, the sensitivity of the model to surface heat and moisture flux depends on the diapycnal diffusivity to the extent that the latter parameter controls the strength of the advective and diffusive processes at equilibrium, and by consequence the strength of their rate of change. Both the strength of the THC and the thickness of the thermocline highly depend on the diapycnal diffusivity. As a consequences also the advective timescale and the magnitude of the GM advective fluxes and both isopycnal and diapycnal fluxes are related to the diapycnal diffusivity. Therefore the relation between sensitivity to surface forcing and diapycnal diffusivity is likely to be an indirect consequence of the relation between the latter parameter and the state of the climate at equilibrium.

The rate of ocean heat uptake under global warming experiments increases with diapycnal diffusivity. The increase in ocean heat content is related to the decrease in bolus velocity (GM) advection and isopycnal diffusion that are the major heat sinks. The role of convection is negligible in this version of the model since first GM advection and then isopycnal diffusion, efficiently mix the surface ocean. At high latitudes, the rise in sea surface temperature due to global warming leads to a decrease of isopycnal slope and in the temperature gradient along isopycnals. Consequently both GM advection and isopycnal diffusion are reduced inducing warming of the subsurface ocean. At equilibrium, the magnitude of these processes is greater for a thicker thermocline, thus for larger diapycnal diffusivity. In global warming experiments the decrease in upward isopycnal diffusion and GM advection is proportional to their value at equilibrium; hence, the rate of ocean heat uptake is larger for larger diapycnal diffusivity.

The uncertainty in the global value of the diapycnal diffusivity reflects on the uncertainty in ocean heat uptake under global warming scenarios, which in turn regulates the increase in surface air temperature (SAT) and sea level rise (SLR). Our calculations suggest that an increase of the diapycnal diffusivity by a factor 10 (from 0.1 to 1.0 $cm^2\ s^{-1}$) leads, at the time of doubling CO_2, to a decrease of SAT of 0.4 K and an increase of SLR due to thermal expansion of 4 cm.

Acknowledgments. We thank the two anonymous reviewers for useful comments and suggestions that improved the clarity of the manuscript. This research was supported in part by MIT's Joint Program on the Science and Policy of Global Change and in part by the Office of Science (BER), U.S. Department of Energy, Grant DE-FG02-93ER61677.

REFERENCES

Bryan, F., 1987: Parameter sensitivity of primitive equation ocean general circulation models. *J. Phys. Oceanogr.,* **17,** 970–985.

Bryan, K., 1984: Accelerating the convergence to equilibrium of ocean–climate models. *J. Phys. Oceanogr.,* **14,** 666–673.

Covey, C., K. M. Achuta Rao, S. J. Lambert, and K. E. Taylor, 2000: Intercomparison of present and future climates simulated by coupled ocean-atmosphere GCMs. PCMDI Rep. 66, 52 pp.

Dalan, F., P. H. Stone, I. V. Kamenkovich, and J. R. Scott, 2005: Sensitivity of the ocean's climate to diapycnal diffusivity in an EMIC. Part I: Equilibrium state. *J. Climate,* **18,** 2460–2481.

Forest, C. E., P. H. Stone, A. P. Sokolov, M. R. Allen, and M. D. Webster, 2002: Quantifying uncertainties in climate system properties with the use of recent climate observations. *Science,* **295,** 113–117.

Ganopolsky, A., V. Petoukhov, S. Rahmstorf, V. Brovkin, M. Claussen, A. Eliseev, and C. Kubatzki, 2001: CLIMBER-2: A climate system model of intermediate complexity. Part II: Model sensitivity. *Climate Dyn.,* **17,** 735–751.

Gent, P. R., and J. C. McWillams, 1990: Isopycnal mixing in ocean circulation models. *J. Phys. Oceanogr.,* **20,** 150–155.

Gregory, J. M., 2000: Vertical heat transports in the ocean and their effect on time-dependent climate change. *Climate Dyn.,* **16,** 501–515.

Hansen, J., G. Russel, D. Rind, P. Stone, A. Lacis, S. Lebedeff, R. Ruedy, and L. Travis, 1983: Efficient three-dimensional global models for climate studies: Model I and II. *Mon. Wea. Rev.,* **111,** 609–662.

Houghton, J. T., Y. Ding, D. J. Griggs, M. Noguer, P. J. van der Linden, X. Dai, K. Maskell, and C. A. Johnson, 2001: *Climate Change 2001: The Scientific Basis*. Cambridge University Press, 881 pp.

Huang, B., P. H. Stone, and C. Hill, 2003a: Sensitivities of deep-ocean heat uptake and heat content to surface fluxes and subgrid-scale parameters in an ocean general circulation model with idealized geometry. *J. Geophys. Res.,* **108,** 3015, doi:10.1029/2001JC001218.

——, ——, A. P. Sokolov, and I. V. Kamenkovich, 2003b: The deep-ocean heat uptake in transient climate change. *J. Climate,* **16,** 1352–1363.

——, ——, ——, and ——, 2003c: Ocean heat uptake in transient climate change: Mechanisms and uncertainty due to subgrid-scale eddy mixing. *J. Climate,* **16,** 3344–3356.

Huang, R. X., 1999: Mixing and energetics of the oceanic thermohaline circulation. *J. Phys. Oceanogr.,* **29,** 727–746.

Hughes, T. C. M., and A. J. Weaver, 1994: Multiple equilibria of an asymmetric two-basin ocean model. *J. Phys. Oceanogr.,* **24,** 619–637.

Jiang, S., P. H. Stone, and P. Malanotte-Rizzoli, 1999: An assessment of the Geophysical Fluid Dynamics Laboratory ocean model with coarse resolution: Annual-mean climatology. *J. Geophys. Res.,* **104,** 25 623–25 645.

Kamenkovich, I. V., A. P. Sokolov, and P. H. Stone, 2002: An efficient climate model with a 3D ocean and a statistical-dynamical atmosphere. *Climate Dyn.,* **19,** 585–598.

——, ——, and ——, 2003: Feedbacks affecting the response of the thermohaline circulation to increasing CO_2: A study with a model of intermediate complexity. *Climate Dyn.,* **21,** 119–130.

Knutti, R., and T. F. Stocker, 2002: Limited predictability of the future thermohaline circulation close to an instability threshold. *J. Climate,* **15,** 179–186.

Ledwell, J. R., E. T. Montgomery, K. L. Polzin, L. C. St. Laurent, R. W. Schmitt, and J. M. Toole, 2000: Evidence for enhanced mixing over rough topography in the abyssal ocean. *Nature,* **403,** 179–182.

Manabe, S., and R. J. Stouffer, 1999: Are two modes of thermohaline circulation stable? *Tellus,* **51A,** 400–411.

Marotzke, J., 1997: Boundary mixing and the dynamics of three-dimensional thermohaline circulation. *J. Phys. Oceanogr.,* **27,** 1713–1728.

Munk, W., and C. Wunsch, 1998: Abyssal recipes II: Energetics of tidal and wind mixing. *Deep-Sea Res.,* **45,** 1977–2010.

Pacanowski, R. C., 1996: MOM2 version 2.0: Documentation user's guide and reference manual. Geophysical Fluid Dynamics Laboratory Tech. Rep. 3.2, 232 pp.

Park, Y. G., and K. Bryan, 2000: Comparison of thermally driven circulations from a depth-coordinate model and an isopycnal-layer model. Part I: Scaling-law sensitivity to vertical diffusivity. *J. Phys. Oceanogr.,* **30,** 590–605.

Polzin, K. L., J. M. Toole, J. R. Ledwell, and R. W. Schmitt, 1997: Spatial variability of turbulent mixing in the abyssal ocean. *Science,* **276,** 93–96.

Prinn, R., and Coauthors, 1999: Integrated global system model for climate policy assessment: Feedbacks and sensitivity studies. *Climatic Change,* **41,** 469–546.

Redi, M. H., 1982: Oceanic isopycnal mixing by coordinate rotation. *J. Phys. Oceanogr.,* **12,** 1154–1158.

Sokolov, A. P., and P. H. Stone, 1998: A flexible climate model for use in integrated assessments. *Climate Dyn.,* **14,** 291–303.

——, C. E. Forest, and P. H. Stone, 2003: Comparing oceanic heat uptake in AOGCM transient climate change experiments. *J. Climate,* **16,** 1573–1582.

Stocker, T. F., and A. Schmittner, 1997: Influence of CO_2 emissions rates on the stability of the thermohaline circulation. *Nature,* **388,** 862–865.

Stone, P. H., and M.-S. Yao, 1990: Development of a two-dimensional zonally averaged statistical–dynamical model. Part III: The parameterization of the eddy fluxes of heat and moisture. *J. Climate,* **3,** 726–740.

Thorpe, R. B., J. M. Gregory, T. C. Johns, R. A. Woods, and J. F. B. Mitchell, 2001: Mechanisms determining the Atlantic thermohaline circulation response to greenhouse gas forcing in a non-flux-adjusted coupled climate model. *J. Climate,* **14,** 3102–3116.

Webster, M., and Coauthors, 2003: Uncertainty analysis of climate change and policy response. *Climatic Change,* **61,** 295–320.

Zhang, J., R. W. Schmitt, and R. X. Huang, 1999: The relative influence of diapycnal mixing and hydrologic forcing on the stability of the thermohaline circulation. *J. Phys. Oceanogr.,* **29,** 1096–1108.